SHROUDED IMPELLER TEST PROGRAM

William J. McAnally, III, et al

Pratt and Whitney Aircraft

Prepared for:

Army Air Mobility Research and Development Laboratory

July 1974

EUSTIS DIRECTORATE POSITION STATEMENT

The purpose of the program was to test a single-stage centrifugal compressor using existing hardware including a mechanically proven shrouded impeller. Although the performance of the shrouded impeller was poorer than anticipated, the technical objectives of the program were met. Because of the limited scope of the technical effort, further redesign, rematching, and testing were not initiated to improve the performance of the machine.

This report has been reviewed by technical personnel of this Directorate, and the Directorate agrees with the conclusions contained herein.

The U. S. Army project engineers for this effort were R. A. Langworthy and Paul F. Haley, Technology Applications Division.

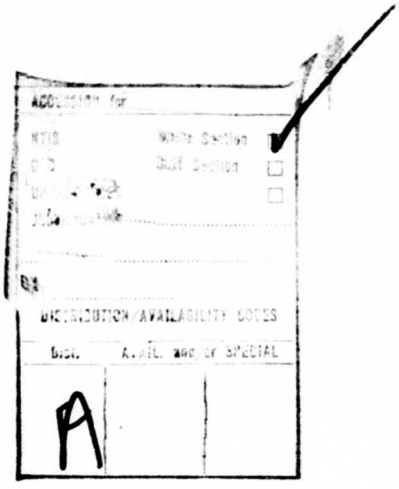

DISCLAIMERS

The findings in this report are not to be construed as an official Department of the Army position unless so designated by other authorized documents.

When Government drawings, specifications, or other data are used for any purpose other than in connection with a definitely related Government procurement operation, the United States Government thereby incurs no responsibility nor any obligation whatsoever; and the fact that the Government may have formulated, furnished, or in any way supplied the said drawings, specifications, or other data is not to be regarded by implication or otherwise as in any manner licensing the holder or any other person or corporation, or conveying any rights or permission, to manufacture, use, or sell any patented invention that may in any way be related thereto.

Trade names cited in this report do not constitute an official endorsement or approval of the use of such commercial hardware or software.

DISPOSITION INSTRUCTIONS

Destroy this report when no longer needed. Do not return it to the originator.

UNCLASSIFIED

SECURITY CLASSIFICATION OF THIS PAGE (When Data Entered)

REPORT DOCUMENTATION PAGE		READ INSTRUCTIONS BEFORE COMPLETING FORM
1. REPORT NUMBER USAAMRDL-TR-74-46	2. GOVT ACCESSION NO.	3. RECIPIENT'S CATALOG NUMBER AD-784133
4. TITLE (and Subtitle) SHROUDED IMPELLER TEST PROGRAM		5. TYPE OF REPORT & PERIOD COVERED Final Report 6. PERFORMING ORG. REPORT NUMBER FR-6328
7. AUTHOR(s) William J. McAnally, III and Jimmy D. Goodrum		8. CONTRACT OR GRANT NUMBER(s) DAAJ02-74-C-0001
9. PERFORMING ORGANIZATION NAME AND ADDRESS Pratt & Whitney Aircraft Division United Aircraft Corporation Florida Research and Development Center West Palm Beach, Florida 33402		10. PROGRAM ELEMENT, PROJECT, TASK AREA & WORK UNIT NUMBERS Task 1G162207AA7102
11. CONTROLLING OFFICE NAME AND ADDRESS Eustis Directorate, U. S. Army Air Mobility Research and Development Laboratory Fort Eustis, Va. 23604		12. REPORT DATE July 1974 13. NUMBER OF PAGES 85
14. MONITORING AGENCY NAME & ADDRESS(if different from Controlling Office)		15. SECURITY CLASS. (of this report) Unclassified 15a. DECLASSIFICATION/DOWNGRADING SCHEDULE

16. DISTRIBUTION STATEMENT (of this Report)

Approved for public release; distribution unlimited.

17. DISTRIBUTION STATEMENT (of the abstract entered in Block 20, if different from Report)

18. SUPPLEMENTARY NOTES

19. KEY WORDS (Continue on reverse side if necessary and identify by block number)

Impellers
Pressure
Ratios
Performance (Engineering)
Diffusers

20. ABSTRACT (Continue on reverse side if necessary and identify by block number)

The objectives of the program were to demonstrate the feasibility of using a shrouded impeller in a high-pressure-ratio centrifugal compressor, to determine the performance of the shrouded impeller, and to compare this performance to that of a similar 10:1 pressure ratio conventional open-face impeller previously tested under Contract DAAJ02-70-C-0006. A shrouded impeller offers (1) the potential for reducing friction heating losses caused by relative motion between impeller blades and stationary shroud, (2) the ability to eliminate impeller blade-to-shroud clearance leakage losses, and

DD FORM 1 JAN 73 1473 EDITION OF 1 NOV 65 IS OBSOLETE

UNCLASSIFIED

SECURITY CLASSIFICATION OF THIS PAGE (When Data Entered)

(3) the capability of operating with hub and shroud walls extended beyond the impeller exit to form a rotating vaneless space.

The shrouded impeller was manufactured from a single titanium forging, thereby eliminating blade-to-shroud attachment problems. It was successfully tested to as high as 108% of design speed and over a range of inlet guide vane settings that defined overall and component performance. Although the shrouded impeller demonstrated a reduction in shroud friction heating, overall performance was approximately six percentage points below the design speed efficiency of the conventional open-face impeller. The poor performance was attributed to an apparent hub wall flow separation that occurred within the impeller and caused excessive rotor and diffuser losses and a resultant mismatch between the impeller and diffuser. Current analytical calculations do not predict the hub wall separation that was measured; however, it appears that the separation could be prevented by reducing the height of the impeller exit flow path to reduce the adverse pressure gradient.

TABLE OF CONTENTS

TABLE OF CONTENTS (CONTINUED)

LIST OF ILLUSTRATIONS

LIST OF ILLUSTRATIONS (Continued)

LIST OF ILLUSTRATIONS (Continued)

LIST OF TABLES

INTRODUCTION

The high-pressure-ratio, single-stage centrifugal compressor has been a major element in the Army's continuing effort to simplify and improve the performance of compressors for gas turbine engines in the 2-to-5-lb_m/sec airflow class. Two previous programs that have dealt specifically with conventional, radially bladed centrifugal compressors of 10:1 pressure ratio design have shown the potential for developing the performance required for future small advanced gas turbine engines. The latest 10:1 design, completed and reported by Pratt & Whitney Aircraft under the terms of Contract DAAJ02-70-C-0006*, essentially achieved the design goal of 75% efficiency at 10:1 pressure ratio.

Pratt & Whitney Aircraft analyzed an impeller having an integral shroud rather than a conventional, detached, stationary shroud. This analysis showed that there was the potential for a significant performance improvement (approximately 2-3 points at 10:1 pressure ratio) for a compressor stage incorporating a shrouded impeller. This potential gain in efficiency was attributed to elimination of the clearance leakage losses and the friction heating losses caused by relative motion between the impeller blades and stationary shroud. Although such analyses have been made before, and shrouded impellers are found in high-performance but low-speed centrifugal pumps, the lack of technology to design and fabricate a high-pressure-ratio, high-speed centrifugal compressor with an integral shroud has, in the past, prevented its use. However, improvements in machining techniques for internally contoured surfaces have made the fabrication of an integrally shrouded impeller feasible. To experimentally evaluate this concept, P&WA™ designed a shrouded impeller that is aerodynamically similar to the 10:1 pressure ratio compressor stage tested under Contract DAAJ02-70-C-0006. The entire shrouded impeller was machined from one Ti-6-2-4-6 forging, thereby eliminating shroud-to-blade attachment problems. An additional potential benefit of a shrouded impeller is that the hub and shroud walls can be extended beyond the blade tips to form a rotating vaneless space. To evaluate this additional potential benefit, the shrouded impeller was manufactured with a rotating vaneless space equivalent to the original 10:1 diffuser stationary vaneless space. Prior to initiating this program, the shrouded impeller was spin-pit tested to design speed and mechanically checked out in the compressor rig to 108% of design speed.

The objective of this limited-effort, 5-month program was to experimentally test and determine the performance of the above 10:1 pressure ratio shrouded impeller. Performance is compared with predicted performance and with the performance demonstrated by the conventional compressor tested under Contract DAAJ02-70-C-0006.

*McAnally, III, W. J., 10:1 PRESSURE RATIO SINGLE-STAGE CENTRIFUGAL COMPRESSOR PROGRAM, Pratt & Whitney Aircraft, USAAMRDL Technical Report 74-15, Eustis Directorate, U.S. Army Air Mobility Research and Development Laboratory, Fort Eustis, Virginia, April 1974.

DESIGN

The aerodynamic design of all items in the compressor flow path, with the exception of the impeller and diffuser, was identical to that used in Contract DAAJ02-70-C-0006.

The aerodynamic design of the shrouded impeller was similar to that of the conventional impeller for Contract DAAJ02-70-C-0006 and utilized the same tandem inducer design (although a different piece of hardware). However, the 24 secondary splitter blades in the impeller were removed to facilitate machining the internal flow passages, and the blade thickness distribution was changed to give additional strength at the blade-to-shroud junction. The knee area of the impeller, which was subject to the greatest stresses, had an inverse blade thickness distribution of approximately 0.050 in. on the hub to 0.100 in. on the shroud side. This taper gradually leveled out to a uniform 0.065-in. thickness at the impeller exit. The impeller blade exit diameter was increased 0.060 in. to overcome a loss in pressure ratio attributed to removing the secondary splitters. The hub and shroud of the impeller were extended 0.175 in. radially beyond the blade tip to form a rotating vaneless space in the diffuser entrance that was an integral part of the impeller. A photograph of the shrouded impeller and tandem inducer is shown in Figure 1a. The conventional design impeller is shown in Figure 1b for comparative purposes.

The 32-pipe diffuser was also similar in design to the diffuser tested under Contract DAAJ02-70-C-0006. The diffuser geometry, as presented in Figure 2, was dictated by the physical dimensions of the shrouded impeller and rotating vaneless space and the anticipated impeller exit conditions.

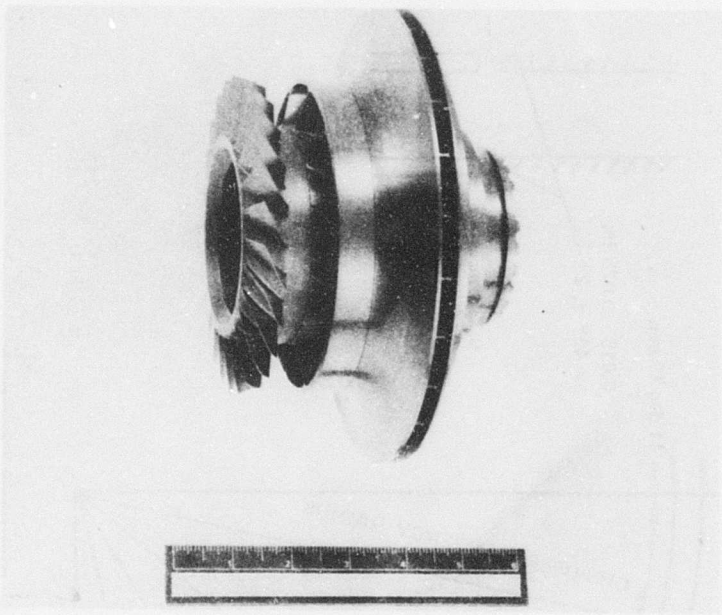

a. P&WA 10:1 PRESSURE RATIO
SHROUDED IMPELLER

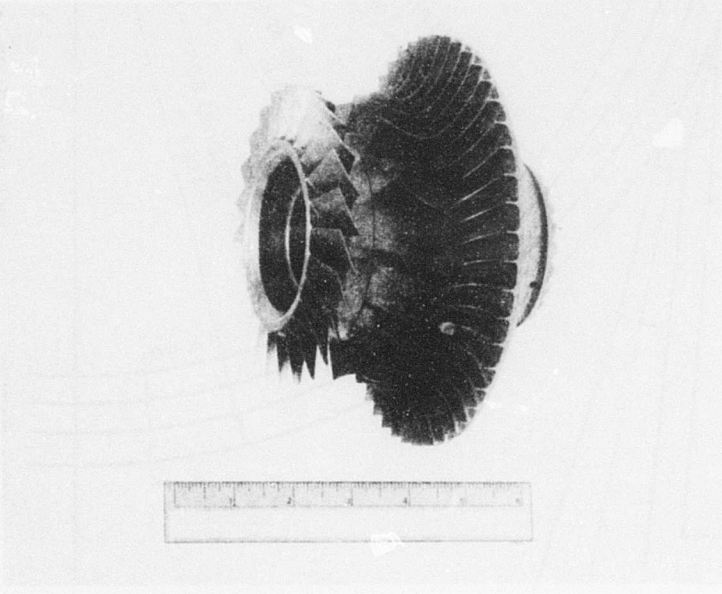

b. CONVENTIONAL DESIGN 10:1 PRESSURE RATIO IMPELLER
FROM CONTRACT DAAJ02-70-C-0006

Figure 1. Comparison of Shrouded Impeller and Conventional Impeller.

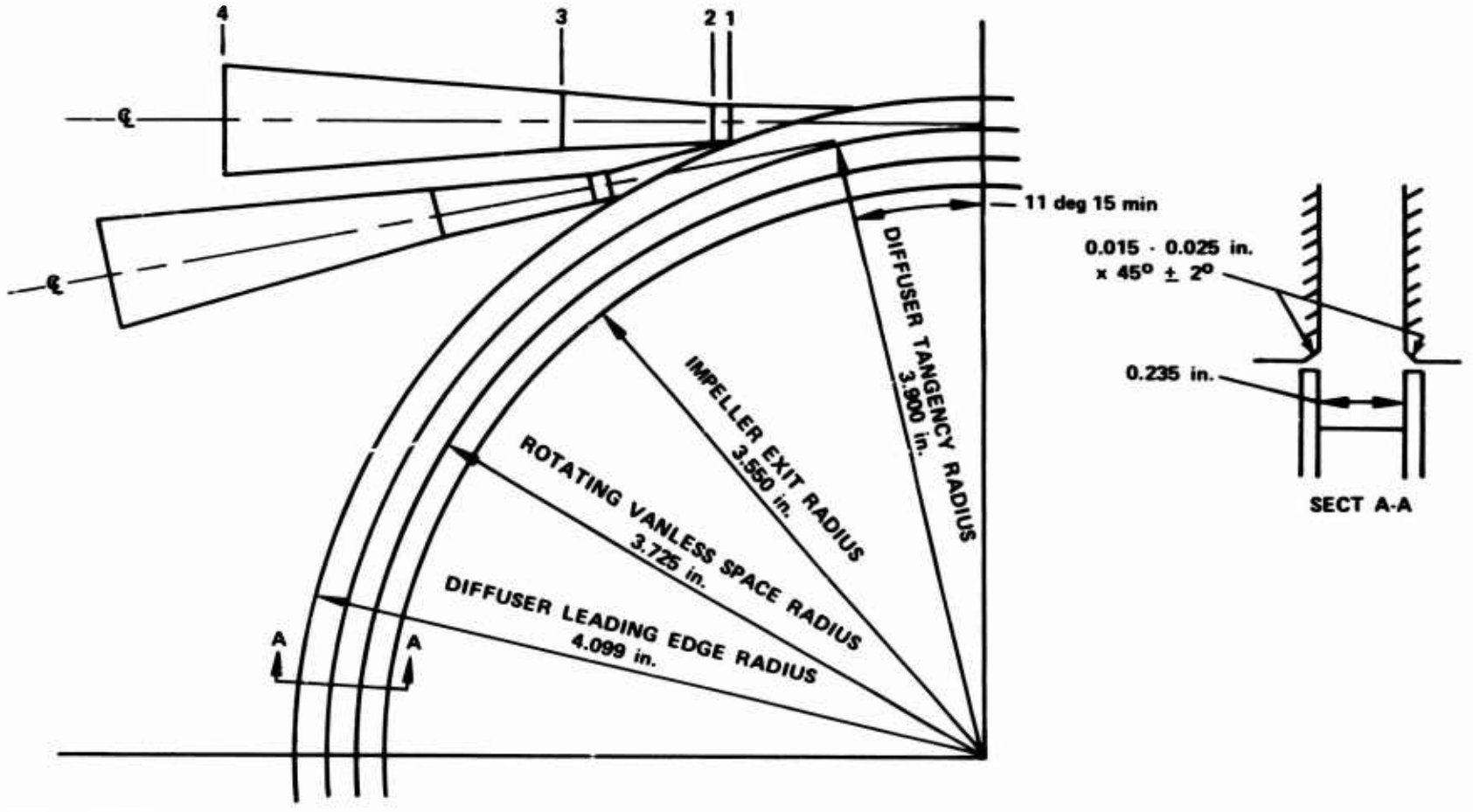

CONE ANGLES:	AREA RATIOS:	PIPE DIAMETERS, in.:	DIFFUSER LENGTH, in.:
1-2 0 deg (ref)	1-2 1.0 (ref)	1&2 - 0.2347	1-2 0.1178
2-3 3 deg (ref)	3-2 1.2452 (ref)	3 - 0.2619	2-3 0.5014
3-4 5 deg (ref)	4-2 3.3614 (ref)	4 - 0.4303	3-4 1.9289

Figure 2. Shrouded Impeller Pipe Diffuser Design.

TEST EQUIPMENT

COMPRESSOR TEST RIG

The compressor research rig incorporated both the compressor and drive turbine on a single rotor. The drive turbine had an integral single entry and a double exit, thus forming a back-to-back configuration. A schematic of the compressor rig is shown in Figure 3; it is the same configuration as that used in Contract DAAJ02-70-C-0006, except that the shrouded impeller and shroud housing were substituted for the conventional impeller and shroud.

The shroud housing incorporated labyrinth seals near the inlet of the shrouded impeller to prevent high-pressure leakage from exceeding 1% of impeller flow. The leakage was restricted from recirculating into the impeller inlet by additional labyrinth seals, and it was collected and measured prior to exhausting to ambient. The axial gap between the stationary inducer shroud and the shrouded impeller was employed for selectively bleeding the inducer shroud boundary layer while testing.

During the assembly of the compressor rig, attention was given to clearance and alignment of the rotating components and balance of the rotor assembly in the cases. A photograph of the shrouded impeller rotor assembly is shown in Figure 4. Positioning of the rotor in the cases was based on preliminary rotor deflections measured in a prior mechanical checkout test. Desired maximum speed rotor clearances were: inducer, 0.005 in.; and impeller labyrinth seals, 0.001 in. The impeller discharge and diffuser were positioned to align their centerlines under running conditions. Final balance of the rotor assembly in the compressor and turbine cases was accomplished within 0.0007 oz-in. unbalance using rivets and pins on each end of the rotor assembly. Post-test check balance values of the rotor assembly indicated up to 0.034 oz-in. unbalance. This balance deterioration was attributed to a 0.001-0.002-in. rub of the inducer blade tips and the silver-plated shroud. The impeller shroud was also lightly rubbed (less than 0.001 in.) by the labyrinth seals; however, the impeller was not damaged and inspection revealed no deformation. Post-test inspection revealed that at maximum speed the impeller and diffuser centerlines were essentially aligned within 0.0014 in.

TEST FACILITIES

A schematic of the P&WA high-speed compressor test facility is shown in Figure 5. The drive turbine was powered by compressor bleed air from a P&WA J75 gas turbine engine. Drive turbine supply air was controlled by two pneumatic valves, one of which was used as vernier control. Since the drive turbine was a radial inflow type and particles in the supply air tend to erode the blade tips, a particle separator was installed downstream of the drive turbine control valves to protect the turbine. Safety systems built into the test facilities included a rapid shutdown system and an abort system. These systems operated automatically when preset conditions were encountered. Table 1 summarizes the initiating actions required to activate the safety controls and the actions taken.

The compressor inlet duct contains a sharp-edged flow measuring orifice, control valve, flow-straightening tubes, and a plenum chamber. An inflatable rubber seal sealed the plenum to the compressor bellmouth. The control valve in the compressor inlet duct remained in a full-open position during all testing.

Inducer bleed flow was scavenged through a system that contained a flow-measuring orifice, a control valve, and a vacuum pump. Compressor performance data were obtained with zero inducer bleed flow at all test conditions. Performance data were also obtained with maximum inducer bleed flow for 8:1 and 10:1 pressure ratio speedlines. Impeller shroud seal leakage mass flow was exhausted through a system that contained a flow-measuring orifice and a control valve. All compressor performance data were obtained with the control valve fully opened and, thus, maximum seal leakage flow.

The compressor exhausted to atmosphere from the diffuser collector through two backpressure control valves, one of which also acted as a vernier control. By controlling the compressor discharge backpressure, it was possible to operate the compressor along a speedline, with transients into and out of stall. A surge relief system was designed and used to detect the onset of surge. The system used a high-frequency-response, pressure-sensing transducer in the diffuser collector. A control module allowed the selection of a rate of change of pressure that would actuate the system. If a higher rate of change of pressure was sensed, a fast-operating valve in the compressor discharge duct was opened. This reduced the compressor backpressure, thereby automatically allowing the compressor to move away from a surge condition.

A pressure control system was used to maintain pressure equilibrium between the impeller hub backface compartment and a buffer seal dam. Most performance data were taken with this delta pressure equal to zero to prevent flow out of or into the flow path at the impeller exit-diffuser entrance. An exception to this condition was when flow was allowed to leak past the impeller backface to determine its effect on the impeller hub exit flow profile.

The required thrust load on the ball bearing was maintained by supplying gaseous nitrogen to the impeller thrust balance cavity through an automatic control valve. This valve was adjustable to any set point and was changed while the rig was in operation.

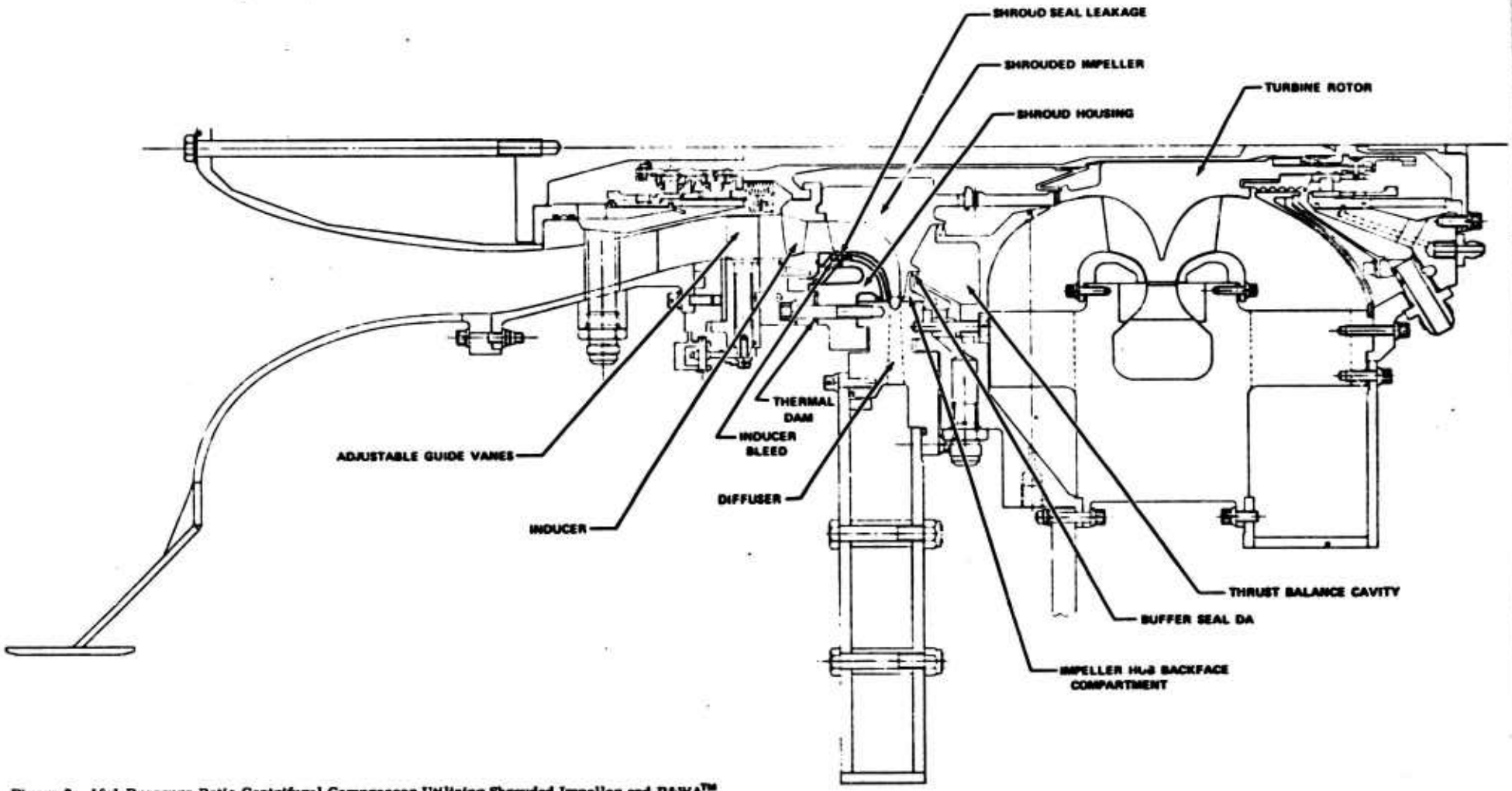

Figure 3. 10:1 Pressure Ratio Centrifugal Compressor Utilizing Shrouded Impeller and P&WA™ Drive Turbine.

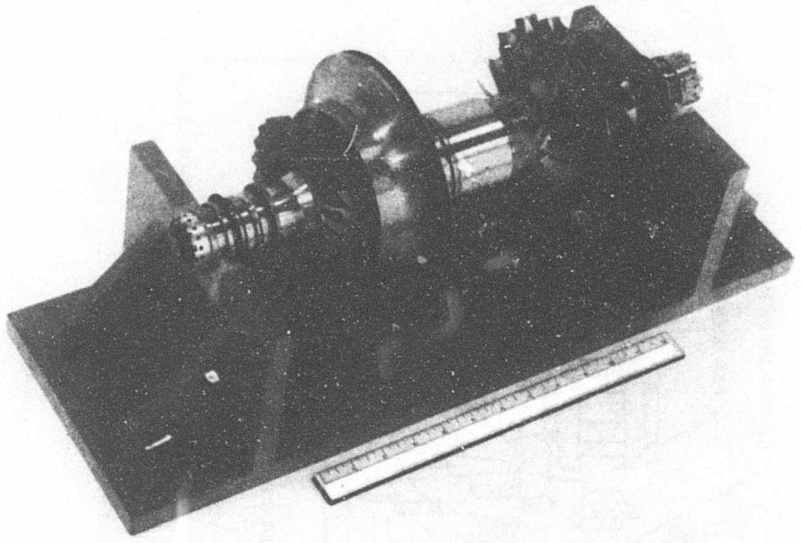

Figure 4. Shrouded Impeller Rotor Assembly.

TABLE 1. TEST FACILITY SAFETY SYSTEMS

Rapid Shutdown System		
Initiating Action	1.	Low thrust balance pressure
	2.	Loss of control room A/C power
Results	1.	Turbine inlet control valves closed
	2.	Compressor discharge valve opened
	3.	Slave engine throttled to idle
Rig Abort System		
Initiating Action	1.	Low lubricating oil supply pressure
	2.	Rotor overspeed
	3.	Manual abort by test engineer
Results	1.	Explosive-actuated turbine inlet valve closed
	2.	If manual abort, turbine inlet manifold vented to ambient
	3.	Turbine inlet control valves closed
	4.	Compressor discharge valve opened
	5.	Slave engine throttled to idle

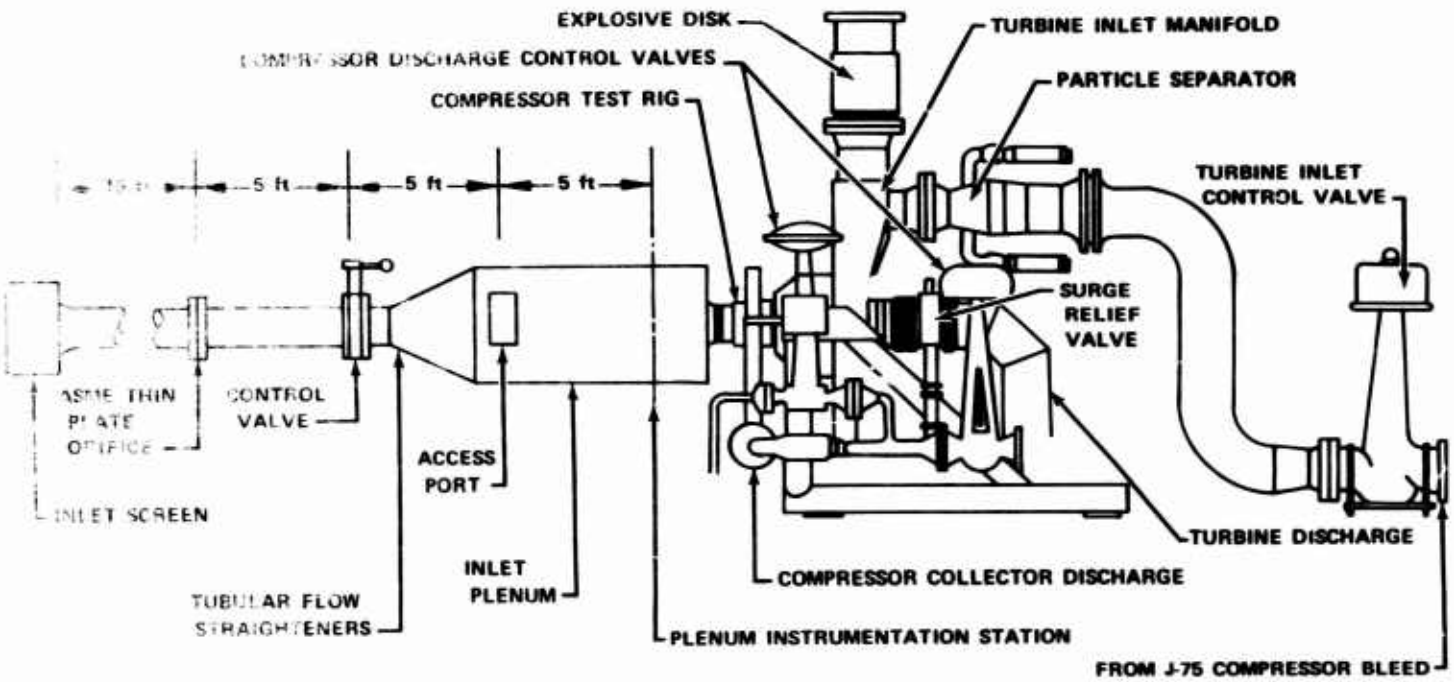

Figure 5. P&WA™ FRDC High-Speed Compressor Test Stand.

INSTRUMENTATION

Instrumentation was provided to permit evaluation of overall and component performance and to monitor rig operation. The instrumentation used to take these data and the instrumentation locations are described herein. Major instrumentation stations for the test compressor are defined in Table 2, and the axial and radial locations of these stations are shown in Figure 6.

TABLE 2. COMPRESSOR INSTRUMENTATION STATIONS

0 - Compressor Inlet-Plenum
1.0 - Inlet Guide Vane Exit
1.5 - Inducer Exit
2.0 - Impeller Exit
3.0 - Diffuser Exit (Collector)

OVERALL PERFORMANCE INSTRUMENTATION

Instrumentation was provided to obtain compressor inlet, inducer bleed, and impeller shroud seal leakage flow rates. Instrumentation was also provided to obtain rotor speed, IGV position, compressor inlet and discharge temperature and pressure, and inducer bleed and impeller seal leakage discharge conditions. These data were combined to define overall performance for the compressor stage. Overall performance instrumentation is described below and is also summarized in Table 3.

Compressor inlet flow rate was calculated from data obtained from a 5.270-in.-diameter thin plate orifice installed upstream of the inlet plenum in a 12.5-in.-diameter inlet duct. (See Figure 5.) The orifice was installed in accordance with ASME standards. Orifice upstream static pressure was measured by means of three static pressure taps, each sensed by a 0- to 15-psia transducer. Three orifice differential static pressures were each sensed by a 5-psid transducer. The temperature of the flow was measured in the inlet plenum.

Inducer bleed and impeller shroud seal leakage flow rates were calculated from data obtained from an orifice in each discharge system. The inducer bleed flow-measuring orifice (0.462-in. diameter) was located in a 0.615-in.-diameter pipe. Orifice upstream static pressure and upstream-downstream differential pressure were sensed by a 0-to-50-psia and a 15-psid transducer, respectively. The 0.274-in.-diameter seal leakage flow-measuring orifice was located in a 0.405-in.-diameter pipe. Orifice upstream static pressure and upstream-downstream differential pressure were sensed by a 0-to-100-psia and a 25-psid transducer, respectively. The temperature of the flow through each orifice was measured by a chromel-alumel (C/A) thermocouple downstream of the orifice.

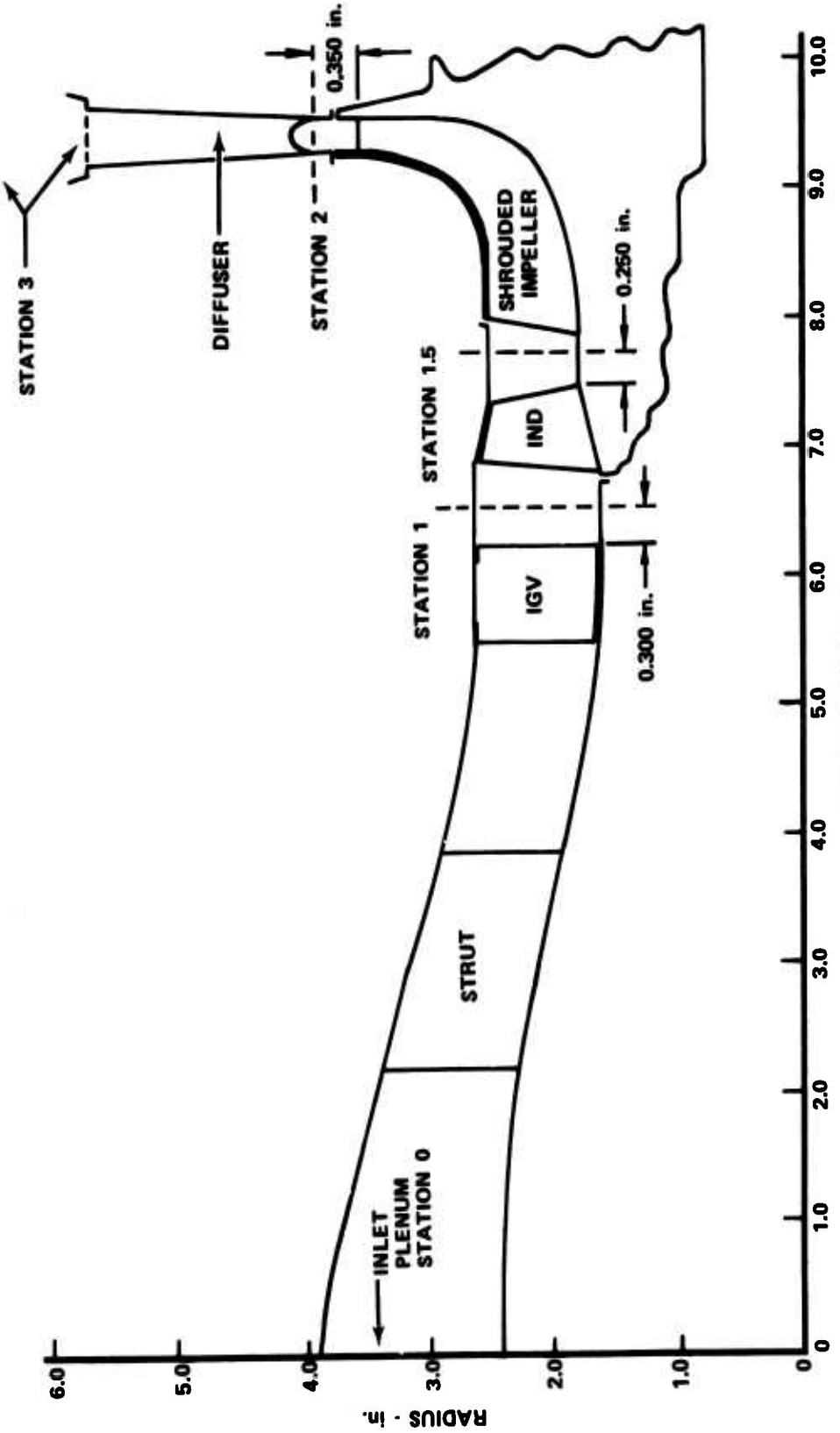

Figure 6. Compressor Flow Path and Instrumentation Station Locations.

TABLE 3. COMPRESSOR OVERALL PERFORMANCE INSTRUMENTATION SUMMARY

Location	Flow Variable	Instrument Type	Quantity
Inlet Duct	P_s	Orifice Wall Tap	3
	ΔP_s	Orifice Wall Tap	3
Plenum	P_t	Kiel Head	3
	T	Rosemount	5
Inlet Guide Vane	α	Potentiometer	1
Inducer Bleed Cavity	P_s	Wall Tap	1
	T	C/A Thermocouple	1
Inducer Bleed Orifice	P_s	Wall Tap	1
	ΔP_s	Upstream-Downstream	1
	T	C/A Thermocouple	1
Shroud Seal Leakage Cavity	P_s	Wall Tap	1
	T	C/A Thermocouple	1
Seal Leakage Orifice	P_s	Wall Tap	1
	ΔP_s	Upstream-Downstream	1
	T	C/A Thermocouple	1
Diffuser Exit	P_t	Rakes	9
Collector	P_s	Wall Tap	7
	T	Aspirated Thermocouple	4
Rotor Speed	Speed	Electromagnetic Pickup	2

Impeller rotational speed was obtained from two electromagnetic pickups mounted adjacent to a six-tooth gear on the rear of the drive turbine rotor shaft. Inlet guide vane position was determined from measurements obtained from a potentiometer connected to the IGV actuator. Compressor inlet total pressure was measured with three Kiel-type total pressure probes located in the inlet plenum and connected to 0- to 15-psia pressure transducers. Compressor inlet total temperature was measured with five Rosemount resistance thermometers installed at various radial positions in the inlet plenum.

Diffuser exit total pressure was measured by means of three total pressure rakes, each consisting of three elements, as shown in Figure 7, and installed at the exit plane of the diffuser tubes. Each element was sensed by a pressure-scanning system using a 0- to 150-psia transducer. The locations of the nine total pressure probes superimposed onto one diffuser tube are shown in Figure 8. It was noted that the center probe of each rake was in the same relative position in each of three tubes to provide redundant measurements at this point. Also shown in Figure 8 are the seven equal areas that were assigned to the total pressures measured by the rakes for mass-averaging purposes.

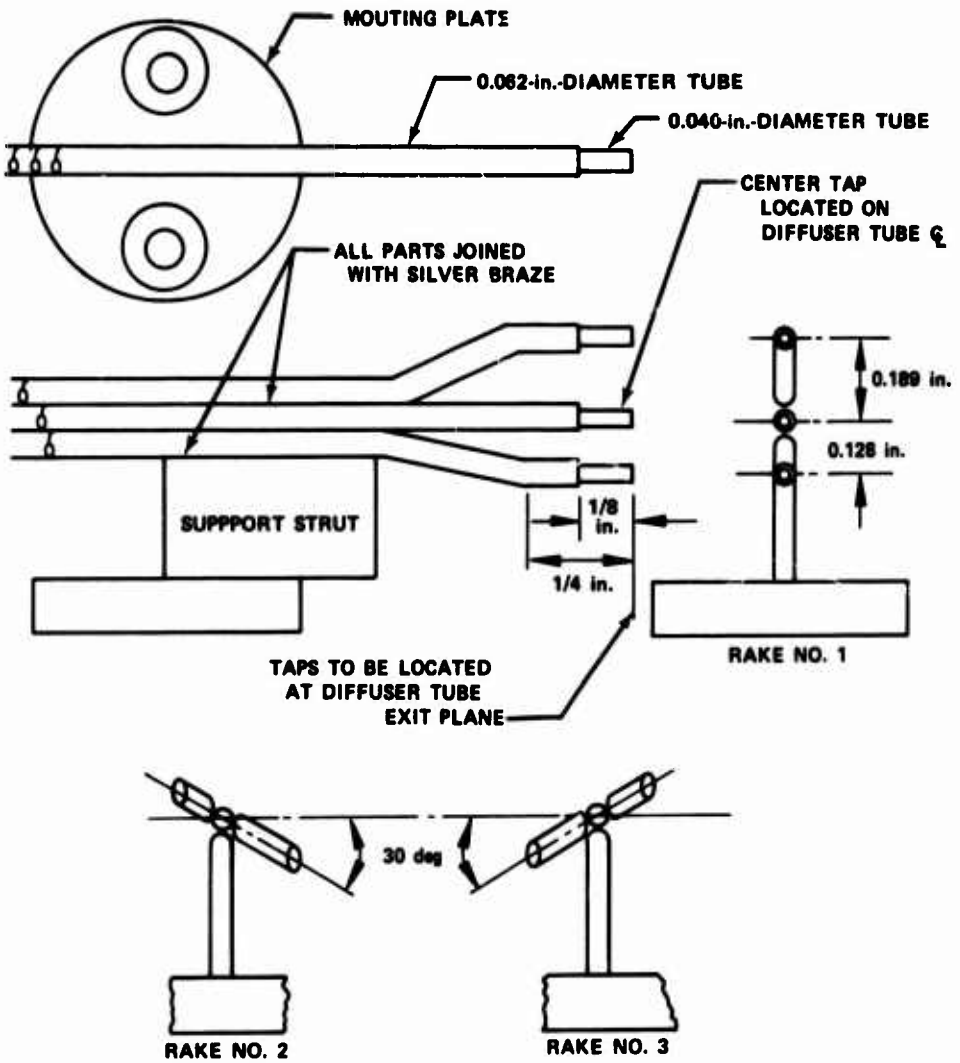

Figure 7. Diffuser Exit Total Pressure Rakes.

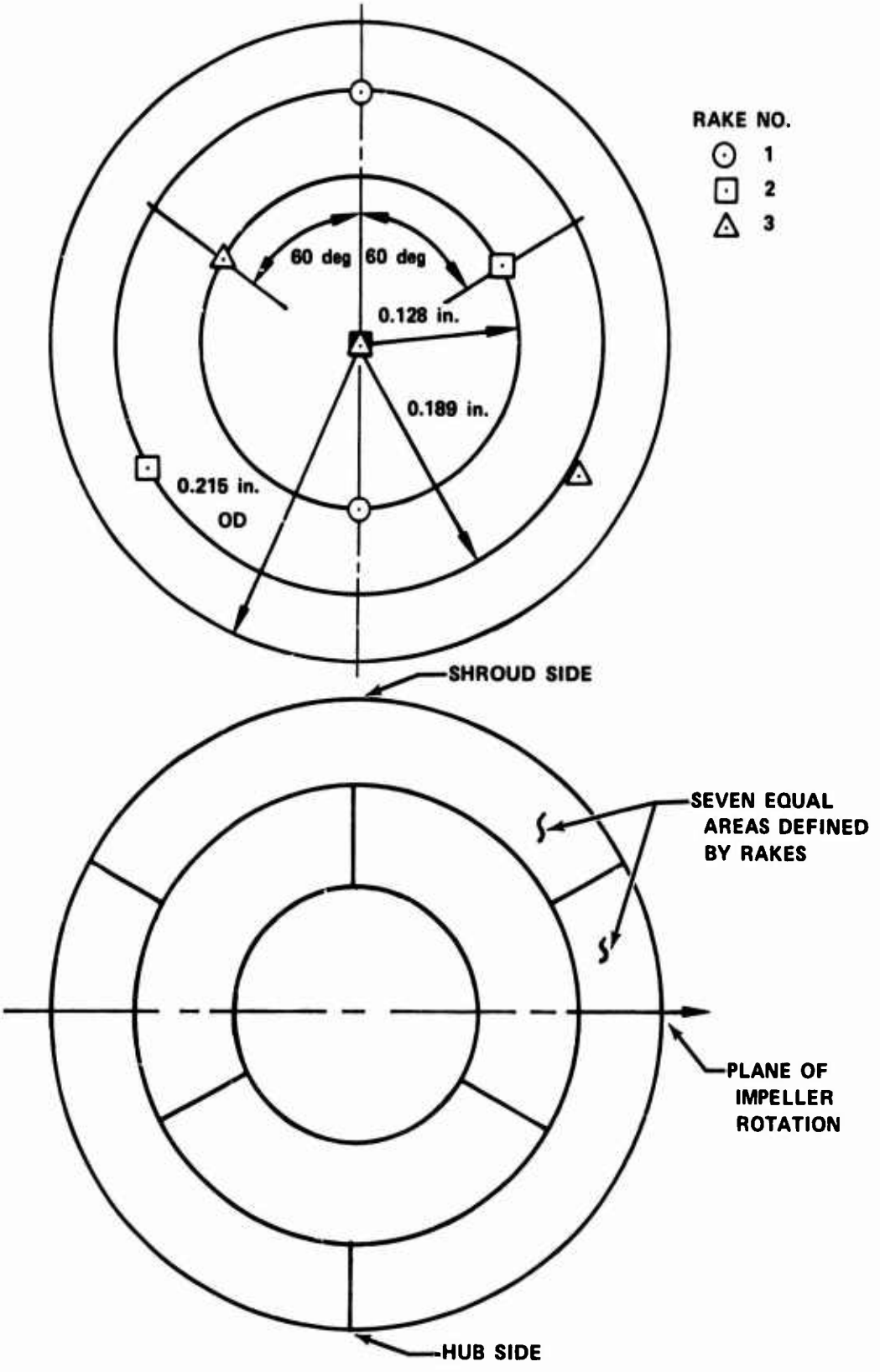

Figure 8. Placement of Total Pressure Probes in Diffuser Exit Plane Station.

Compressor exit static pressure was measured by means of seven static pressure taps in the collector; with six connected to a pressure-scanning system using a 0- to 150-psia transducer, and one connected to a 0-to-200-psia close-coupled transducer for fast response during surges. The taps were located on the shroud-side wall so that neither diffuser discharge velocity nor the collector struts interfered with the measurements. The design and location of these taps are shown in Figure 9. Compressor exit total temperature was measured with four chromel-alumel (C/A) thermocouples in the discharge collector aligned on diffuser pipe centerlines. A tabulation of the pressure tap and thermocouple locations is given in Table 4. Thermocouples were installed at two additional locations; however, their measurements were not used to calculate the average collector temperature. To increase the accuracy of the temperature measurements, the thermocouples were constructed such that the sensor was located in a flow stream that was aspirated to ambient. Figure 10 shows the shielded thermocouples previously used in Contract DAAJ02-70-C-0006 and the new, externally aspirated-type thermocouple. Placement of the sensor in the high velocity flow reduces measurement errors caused by thermal conduction. In addition, the thermocouples were constructed from a single batch of calibrated special-limits-of-error wire. This wire was continuous from the thermocouple junction to the reference junction to eliminate errors caused by connectors and by the lower quality wire normally used between the connector and the reference junction.

The inducer bleed and impeller shroud seal leakage flows were each collected in a manifold inside the compressor cases before being exhausted. The temperature and static pressure of the flow in each manifold was measured by a chromel-alumel (C/A) thermocouple and a static pressure tap sensed by a pressure-scanning transducer.

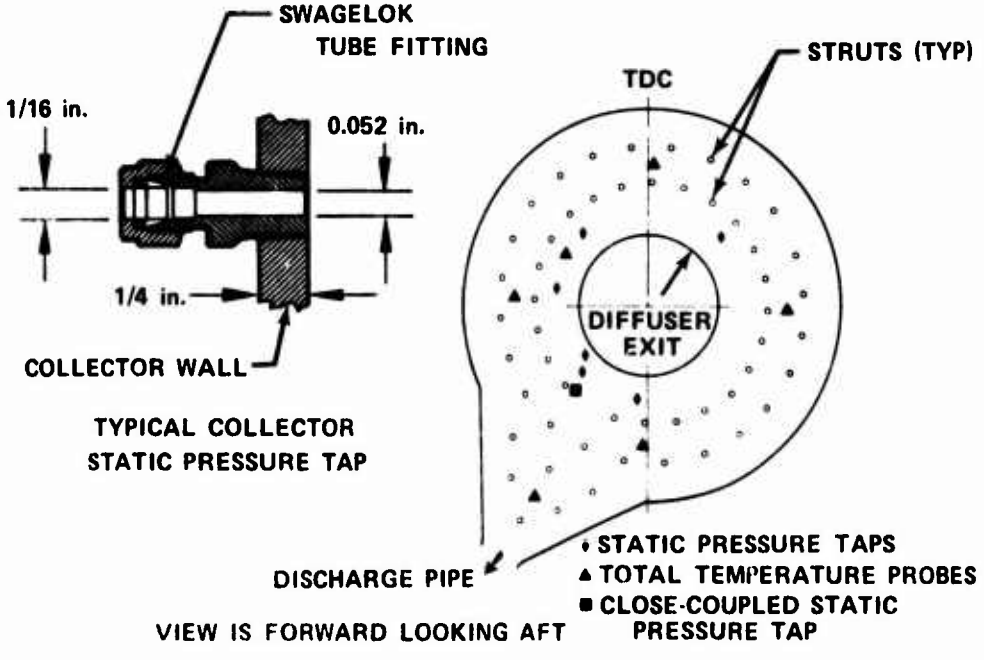

Figure 9. Collector Instrumentation Locations.

TABLE 4. LOCATION OF COLLECTOR INSTRUMENTATION

Probe	Axial Location**	Radial Location, in.	Circumferential Location, deg***
Static Tap			
1	S	7.5	46
2	S	7.5	316
3	S	7.5	281
4	S	6.4	231
5	S	7.5	226
6	S	9	221*
7	S	7.5	181
Thermocouple			
1	M	11.0	3
2	M	11.0	93
3	M	11.0	183
4	M	11.0	273
5	M	7.25	300
6	M	18.25	210

*Connected to close-coupled transducer

**S - Shroud side
M - Midway between collector manifold walls

***Circumferential location is measured clockwise from TDC, forward looking aft. Thermocouples 5 and 6 were not used to calculate average collector temperature.

COMPONENT PERFORMANCE INSTRUMENTATION

Instrumentation was provided to evaluate component performances; namely, that of the inducer, shrouded impeller, and diffuser. The component performance instrumentation is described below and is summarized in Table 5. Static pressure at station 1 was measured by four equally spaced shroud wall taps. Radial distributions of total pressure, total temperature, and air angle at the inducer exit (station 1.5) were obtained by means of a radially traversing cobra probe and thermocouple. The cobra probe and thermocouple are shown in Figure 11. The pressure ports were constructed from 0.020-in.-OD tubing. Additionally, four static pressure taps were equally spaced about the circumference on the shroud wall in the plane of the traversing cobra probe.

Instrumentation was provided to measure impeller tip static pressure on both the shroud side and the hub side, and total pressure and air angle distribution across the flow path at the impeller exit (station 2). Impeller tip static pressure on the shroud side was obtained from measurements of the pressure in a circumferential

passage that is connected with the flow path by a 0.026-in.-wide circumferential groove between the shroud housing and the diffuser. Pressure was measured through four ports that were equally spaced around the circumference. This circumferential groove scheme is shown in Figure 12. Impeller tip backface pressure was measured by means of two 0.062-in.-diameter tubes installed 180 deg apart in the impeller tip backface cavity.

ORIGINAL SHIELDED CONFIGURATION

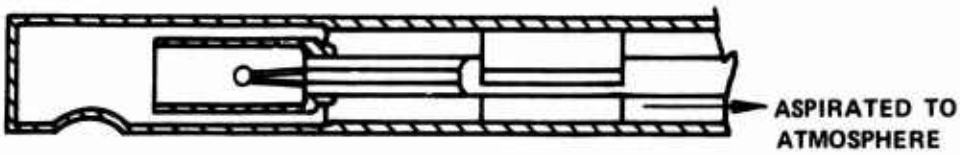

REDESIGNED EXTERNALLY ASPIRATED CONFIGURATION

Figure 10. Original and Redesigned Collector Thermocouples.

TABLE 5. COMPRESSOR COMPONENT PERFORMANCE INSTRUMENTATION SUMMARY

Location	Flow Variable	Instrument Type	Quantity
Station 1	P_s	Shroud Wall Tap	4
Station 1.5	P_s	Shroud Wall Tap	4
	P_t, T, α	Radial Traversing Cobra Probe With Thermocouple	1
Impeller Tip, Shroud Side	P_s	Communicating Groove	4
Impeller Tip, Backface	P_s	Tube	2
Station 2	P_s	Shroud Wall Tap	2
	P_s	Hub Wall Tap	4
	P_t, α	Axial Traversing Cobra Probe	1

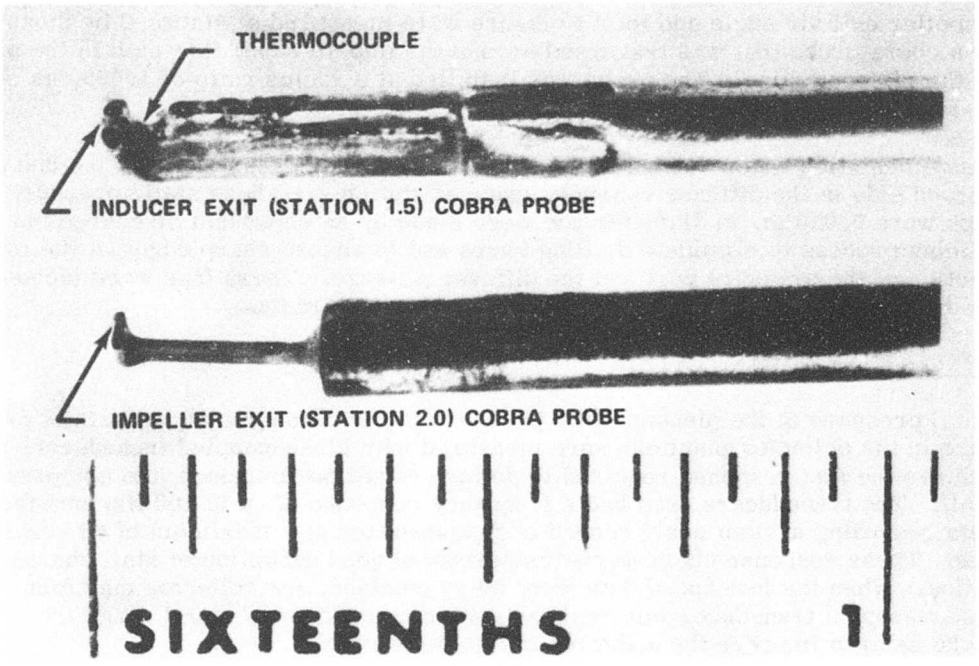

Figure 11. Construction of Traverse Cobra Probes.

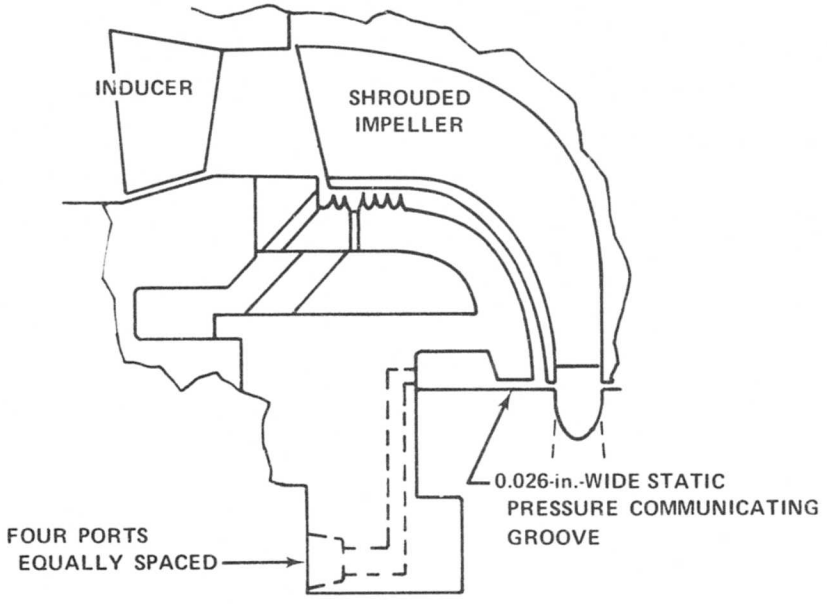

Figure 12. Impeller Tip Static Pressure Passage.

Impeller exit air angle and total pressure were measured at station 2 by means of a cobra probe that was traversed across the impeller exit flow path in the plane of the rig centerline. The probe was installed at a radius ratio of 1.099, as shown in Figure 13.

Instrumentation was provided to measure wall static pressure on both the hub and shroud side in the diffuser vaneless space at station 2. These static pressure taps were 0.020 in. in diameter and were made by an electrical discharge machining process to eliminate drilling burrs and to ensure sharp edges at the intersection of the pressure port and the diffuser passage. These taps were located on diffuser pipe centerlines at diffuser pipe tangency radius.

SPECIAL INSTRUMENTATION

Total pressure in the plenum, total pressure in the diffuser exit, and static pressure in the collector manifold were measured with close-coupled transducers to achieve the fast response required to define overall performance into compressor stall. The transducers used had a frequency response of up to 100 Hz, and the data recording system could record each transducer at a maximum of 65 scans/sec. These response characteristics permitted good definition of stall characteristics. When the low-speed data were being obtained, the collector manifold close-coupled transducer was replaced with a transducer of small range (0-25 psia) to improve the accuracy of the measurement.

DATA READOUT AND RECORDING SYSTEM

All compressor rig data were recorded with an automatic digital magnetic tape recorder. Information needed for safe operation of the rig and for setting data points was displayed in the control room. Control room data readouts included rotor speed, rig vibration levels, bearing temperatures, oil pressure, inlet orifice differential pressure, impeller thrust balance pressure, rig inlet pressure, and rig discharge pressure.

When cobra probe data were being obtained, the total pressure measured by the cobra probe was displayed on an X-Y plotter located adjacent to the traverse actuator controls. This allowed changing the speed, or, if necessary, stopping the cobra probe actuator to allow the probe to respond to changes in the airflow angle.

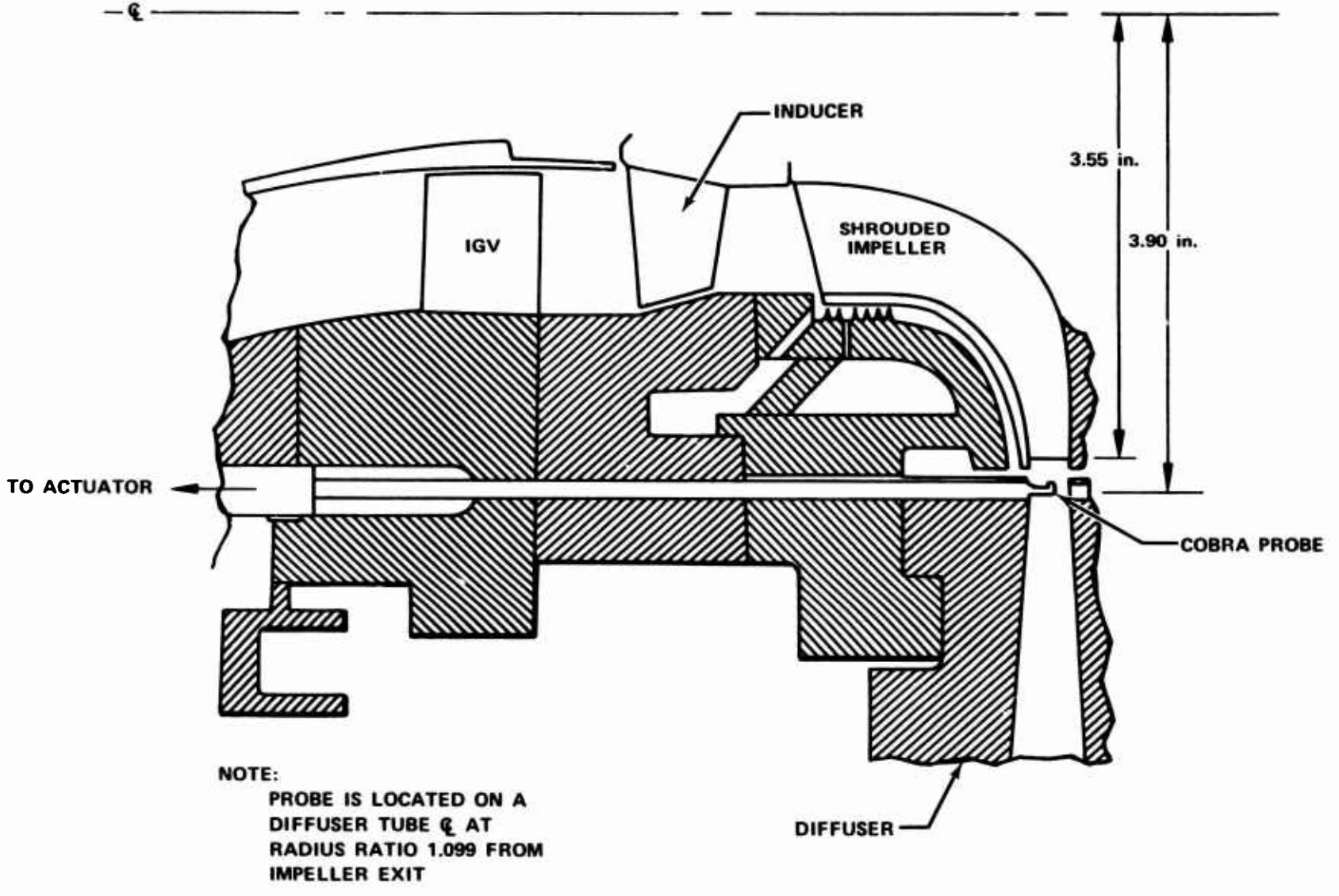

Figure 13. Impeller Exit Cobra Probe Installation.

PROCEDURES

TEST PROCEDURES

Shakedown Test

Prior to the initiation of performance testing, the compressor test rig was subjected to a prerun (nonrotating) checkout of all rig systems and then a shakedown test. The objectives of this checkout and shakedown test were to (1) verify the mechanical integrity of the test rig and (2) check the instrumentation and the data acquisition systems.

During the shakedown test, rig vibrations and bearing temperatures were monitored and rotor radial clearances were measured over the entire range of rig operation. A maximum allowable limit of 270 g's at design speed was set for extended life of the bearings; however, maximum observed vibration levels were only 120 g's. Vibration data were recorded continuously during the test program on analog magnetic tape. Bearing temperatures (180°-220°F) compared favorably with those observed during earlier tests. Bearing temperatures were recorded on a strip chart and on the primary data recording system during the test program.

The inducer blade and impeller inlet shroud radial clearances were measured with mechanical rub probes during the shakedown test. These clearance probes were withdrawn after the impeller rotational speed had reached 70, 85, and 100% of design speed. These measurements indicated adequate clearance; however, inspection of rig hardware after disassembly indicated that an 0.001-0.002-in. inducer tip rub had occurred and that initial measurements used to determine the inducer blade clearance were probably in error.

To determine the scavenge capabilities of the inducer bleed and impeller shroud seal leakage systems, the control valves used to regulate these flows were actuated throughout their full range of operation. Figures 14 and 15 show the maximum inducer bleed and seal leakage system flow capabilities. The inducer bleed is less than 2% of the inlet flow for both the 8:1 and 10:1 pressure ratio speedlines. The labyrinth seal leakage flow is less than 1% of the inlet flow above 1.5 lb_m/sec (75% of design rotor speed).

Adjustments were made to the automatic surge relief system, as necessary, so that it responded to stall-associated pressure fluctuations and not to the gradual pressure changes caused by closing the throttle valves or to random pressure fluctuations.

All instrumentation was checked for continuity from the test rig back to the data recording system. Just prior to the start of each run, all transducer and thermocouple output voltages were calibrated over their operating ranges, and a set of ambient readings was recorded for all the instrumentation for comparison to true ambient conditions. During the shakedown test, overall performance, component performance, and transient data were obtained and processed through the data reduction system to determine if all the instrumentation were recording properly and to check the data acquisition and reduction systems.

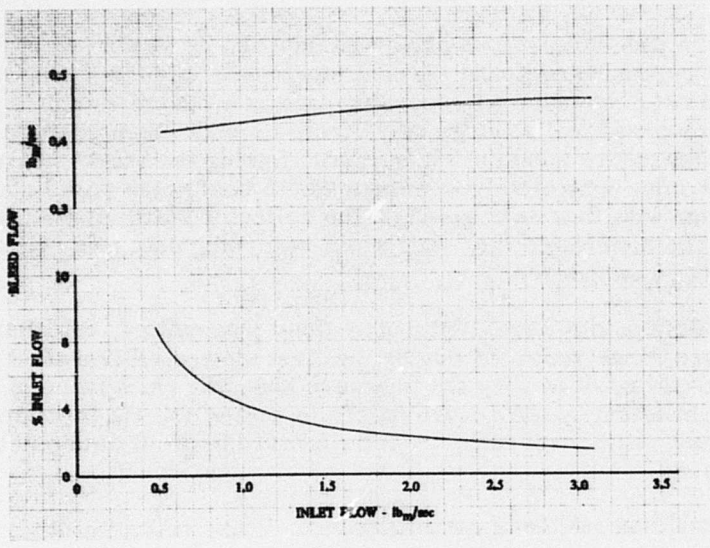

Figure 14. Inducer Bleed Flow Rate Capability.

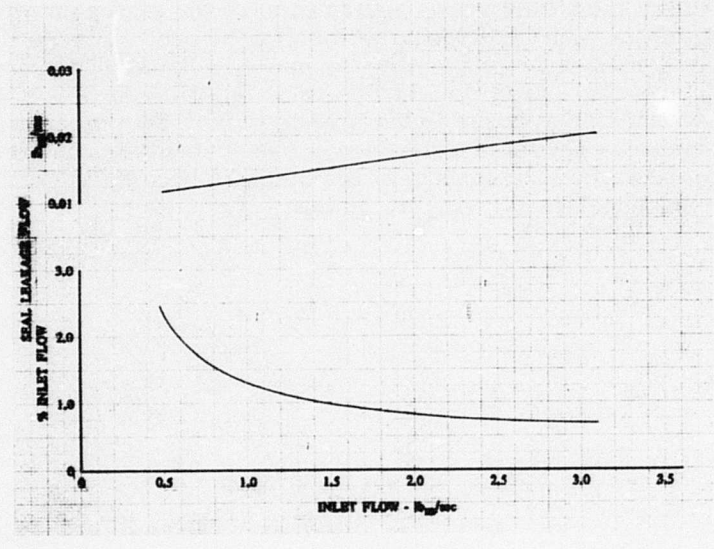

Figure 15. Shroud Seal Leakage Flow Rate Capability.

Overall Performance Data Acquisition

Each speedline was defined by a stall transient and by steady-state points at near-stall, wide-open discharge, and several intermediate points. Slow-stall transients were first performed by recording data at a rate of 1 scan/sec, while closing the compressor discharge valve from its wide-open position, thus increasing backpressure until the rig surged. During the transient, adjustments to the turbine inlet control valves were made to hold rotor speed constant. A near-stall point was then set, based on the collector static pressure, and the compressor again operated into stall while recording data at a higher scan rate, approximately 65 scans/sec.

Steady-state data points were distributed along a speedline, based on the collector static pressure range recorded during the first slow-stall transient. A steady-state point consisted of cycling the pressure scanning units twice at a rate of 2 ports/sec, followed by the recording of the rest of the rig instrumentation for 10 sec at a rate of 10 scans/sec. A detailed outline of all data points taken is shown in Table 6.

Component Performance Data Acquisition

Component performance data were obtained by traversing an air angle, total pressure, and total temperature probe at the inducer exit and an air angle and total pressure probe at the impeller exit. The data recording rate for all traverses was 1 scan/sec.

Inducer exit radial traverses were performed near the stall point on each speedline at 80% of design speed and above by running the probe into its limit and then recording data, while slowly retracting the probe back out of the flow path. Impeller exit traverse data were obtained on each speedline at 80% of design speed and above at the maximum possible backpressure with the traverse probe in the flow path. Data were recorded while slowly traversing the probe from the hub wall back into the shroud. A steady-state point was recorded to coincide with each inducer and impeller exit traverse point.

TABLE 6. SUMMARY OF PERFORMANCE TEST DATA POINTS

Condition		Type of Data			
Speed, % of Design	IGV Prewhirl	Stall Transient	Steady State	Inducer Traverse	Impeller Traverse
(With Inducer Bleed)					
101	-4	1	6	1	2
101	0	2*	6*	1	2
101	10	1	5	1	1
96	0	1	7	1	3
96	10	1	9	1	3
96	20	2	5	2	1
(Without Inducer Bleed)					
101	-4	1	7	1	3
101	0	2*	7	1	4*
101	10	1	5	1	1
96	0	1	7	1	3
96	10	1	5	1	1
96	20	1	5	1	1
90	0	1	5	1	1
90	10	1	6	1	2
90	20	1	6	1	1
85	20	1	6	1	2
80	20	1	6	1	2
70	20	1	6		
50	20	1	6		
30	30	2	7		
20	30	2	7		
10	30	2	8		

*With Impeller Exit Hub Wall Bleed

DATA REDUCTION PROCEDURES

The reduction of data was accomplished in two steps: (1) reduction of overall performance data; and (2) calculation of component performance and velocity triangles. All performance data except orifice and plenum data were corrected to standard day inlet conditions as follows:

$$\text{Corrected pressure} = \frac{\text{recorded pressure}}{\delta}$$

$$\text{Corrected temperature} = \frac{\text{recorded temperature}}{\theta}$$

Overall Performance

The reduction of overall performance data was accomplished through the use of an IBM 360-75 computer program. Actual inlet orifice weight flow, seal leakage weight flow, and inducer bleed weight flow were calculated from orifice equations of the form

$$W_{act} = K_1\left[C - K_2\left(\frac{\Delta P_s}{P_s}\right)\right]\left[\frac{P_s \bullet \Delta P_s}{T}\right]^{1/2} \qquad (1)$$

where

P_s = upstream orifice static pressure (psia)
ΔP_s = orifice differential static pressure (psid)
T = orifice flow total temperature (°R)
C, K_1, K_2 = constants defined for each orifice

Both weight flow and rotor speed were corrected to standard day inlet conditions as follows:

$$W = W_{act}\frac{\sqrt{\theta}}{\delta} \qquad (2)$$

$$N_{cor} = \frac{N_{act}}{\sqrt{\theta}} \qquad (3)$$

The net compressor weight flow was defined as follows:

$$W_{net} = W_o - W_{bl} - W_{sl} \qquad (4)$$

Overall temperature ratio and total-to-static pressure ratio are given, respectively, by

$$TR = T_3/518.688$$

$$PR = P_3/14.696$$

A "flow path" adiabatic efficiency that does not account for the inducer bleed and shroud seal leakage flows was defined as

$$\eta_{flow} = \frac{\text{ideal (isentropic) enthalpy change}}{\text{actual enthalpy change}} = \frac{\Delta hf(PR)}{\Delta hf(TR)} \tag{5}$$

where: $\Delta hf(PR)$ and $\Delta hf(TR)$ were determined by fourth degree curve fits of change in enthalpy vs pressure ratio and temperature ratio data from Table 1 (Dry Air Tables) in Keenan and Kaye Gas Tables. The net adiabatic efficiency, which accounts for the work done on the bleed and seal leakage flows, is given by

$$\eta_{net} = \frac{W_{net} \cdot \Delta hf(PR)}{W_{net} \cdot \Delta hf(TR) + W_{bl} \cdot \Delta hf(TR_{bl}) + W_{sl} \cdot \Delta hf(TR_{sl})} \tag{6}$$

where

$$TR_{bl} = T_{bl}/518.688$$

$$TR_{sl} = T_{sl}/518.688$$

T_{bl} and T_{sl} = the temperatures of the bleed and seal leakage flows, respectively.

At steady-state points the overall pressure ratio was based on the arithmetic average of six collector static pressure taps read through a pressure-scanning system. During stall transients, the pressure ratio was determined from a single collector static pressure tap read through a close-coupled pressure transducer.

Inlet Guide Vane Performance

Inlet guide vane performance, in terms of total pressure loss and turning distribution vs inlet weight flow and guide vane setting, was assumed equal to the inlet guide vane performance demonstrated under Contract DAAJ02-70-C-0006, since the same vanes and inlet system were used.

Inducer Performance

Total pressure, total temperature, air angle, and radial travel data from each inducer traverse were input into an IBM 1130 digital computer program. A constant spanwise static pressure distribution equal to the measured shroud static pressure was assumed.

The ratio of specific heats (γ) was determined from a curve fit of γ vs static temperature (T_s) data and involved an iteration on the value of T_s to satisfy the following at each percent span:

$$\frac{P_t}{P_s} = \left(\frac{T}{T_s}\right)^{\gamma/\gamma-1} \tag{7}$$

The absolute Mach No. (M) was calculated by iterating on the value of M until

$$\frac{P_t}{P_s} = \left(1 + \frac{\gamma - 1}{2} M^2\right)^{\gamma/\gamma - 1} \tag{8}$$

The local speed of sound was calculated by

$$a = (\gamma G R T_s)^{1/2} \tag{9}$$

Total temperatures were corrected for Mach No. effects by dividing the recorded temperatures by a recovery factor. The recovery factor used in the calculations was a linear approximation of the actual probe recovery factor vs Mach No. calibration data. Total pressure and total temperature were then mass-averaged across the span. The mass-average of any quantity (X) is given by

$$\overline{X} = \sum_{i=1}^{n} \Delta W \cdot X \Big/ \sum_{i=1}^{n} \Delta W \tag{10}$$

where

$$\Delta W = \frac{k \cdot \Delta A \cdot P_t}{\sqrt{T}} \sin \alpha$$

The sum of the incremental weight flows from the mass-averaging routine was checked against the corresponding inlet orifice flow, and an iteration was performed on the air angle values until the two flow calculations agreed. This air angle check was necessary because errors of 1 or 2 deg in the alignment of the air angle traverse probes on the test stand are not uncommon. Final mass-average total pressure ($\overline{P}_{t1.5}$) and total temperature ($\overline{T}_{1.5}$) values were then calculated, based on the adjusted air angle profile. Inducer pressure ratio and temperature ratio were calculated as follows:

$$PR_{(1\text{-}1.5)} = \overline{P}_{t1.5} / \overline{P}_{t1} \tag{11}$$

$$TR_{(1\text{-}1.5)} = \overline{T}_{1.5} / 518.688 \tag{12}$$

Inducer efficiency was calculated by the same methods as the overall efficiency and is given by

$$\eta_{ind} = \frac{\Delta hf(PR_{1\text{-}1.5})}{\Delta hf(TR_{1\text{-}1.5})} \tag{13}$$

From M, a, and α the components of the velocity triangles, as defined below, at each percent span were then calculated.

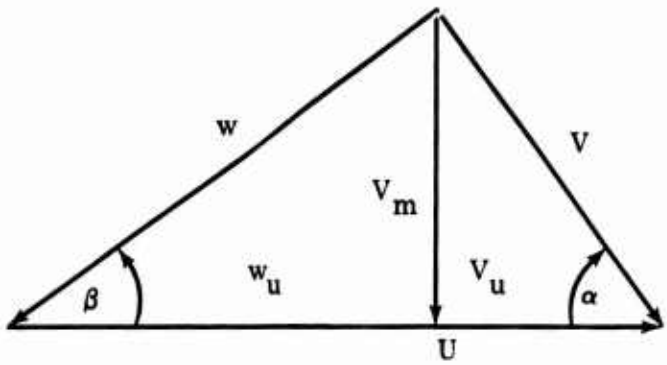

Impeller incidence (i) was determined at each percent span by

$$i = \beta^* - \beta$$

where β^* is the impeller leading-edge metal angle at the corresponding percent span.

Impeller Performance

Impeller exit traverse data were reduced by nearly the same methods as the inducer exit data. Static pressure was assumed to vary linearly between the measured values at the hub and shroud. Total temperature was assumed constant across the passage and equal to the collector total temperature.

Flow at the impeller exit was supersonic across much of the passage at the higher speed points that would cause a shock to form in front of the traverse probe. For data taken where the local value of P_t/P_s was less than 1.893, the flow was assumed subsonic and impeller performance parameters and velocity triangles were calculated as in the inducer section. For values of P_t/P_s greater than 1.893, the flow was assumed supersonic, and a shock correction procedure was incorporated assuming a normal shock to determine the upstream flow conditions.

The mass-average radial velocity ($\overline{V}_m$) and mass-average tangential velocity ($\overline{V}_u$) were calculated, and from these a mass-average air angle was determined:

$$\overline{\alpha}_2 = \tan^{-1}\left(\frac{\overline{V}_m}{\overline{V}_u}\right) \qquad (14)$$

The slip factor at the instrumentation station was calculated by:

$$\text{slip factor} = \frac{\overline{V}_u}{U}$$

The slip factor at the actual impeller tip was determined by using the calculated wheel tip speed (U) and converting the tangential velocity (V_u) derived from measurements at the instrumentation plane to the impeller tip by ratioing by the tip diameter/instrumentation plane diameter, which is the assumption of constant angular momentum. No friction loss was assumed in this calculation. Impeller efficiency was calculated from:

$$\eta_{imp} = \frac{\Delta hf(PR_{1.5-2})}{\Delta hf(TR_{1.5-2})} \tag{15}$$

Combined inducer-impeller (rotor) efficiency was also defined and is given in terms of "flow path" efficiency and net efficiency as follows:

$$(\eta_{\text{rotor}})_{flow} = \frac{\Delta hf(PR_{1-2})}{\Delta hf(TR_{1-2})} \tag{16}$$

$$(\eta_{rotor})_{net} = \frac{(W_o - W_{bl}) \cdot \Delta hf(PR_{1-2})}{(W_o - W_{bl}) \cdot \Delta hf(TR_{1-2}) + W_{bl} \cdot \Delta hf(TR_{bl})} \tag{17}$$

The impeller front face shroud friction temperature rise was calculated from an energy balance equation for the compressor rotor with no inducer bleed:

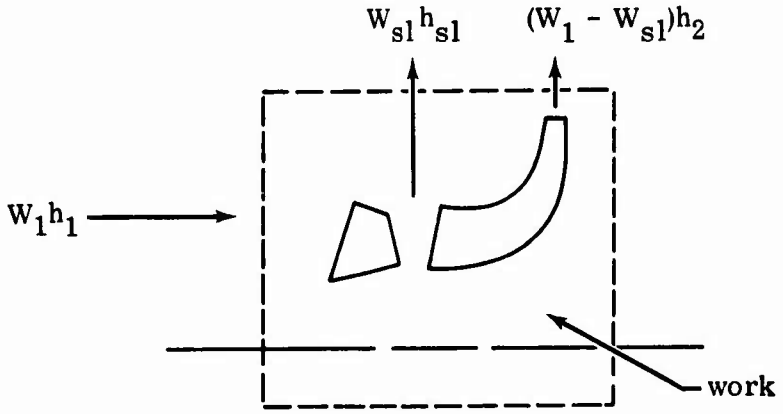

$$W_1 h_1 + \text{work} = W_{sl} h_{sl} + (W_1 - W_{sl}) h_2 \tag{18}$$

The total work was defined as the sum of the Euler work ($W_1 \Delta h_E$) and the front face shroud friction work ($W_1 \Delta h_{sf}$), where:

$$\Delta h_E = \frac{U_2 V_{u2} - U_1 V_{u1}}{GJ} \tag{19}$$

and U and V_u are mean values. Putting the above work terms into the energy balance equation and rearranging yields the following expression for the Δh due to shroud friction:

$$\Delta h_{sf} = \frac{W_{s1}}{W_1} (h_{s1} - h_2) + (h_2 - h_1) - \Delta h_E \tag{20}$$

For the open face impeller configuration this simplifies to:

$$\Delta h_{sf} = (h_2 - h_1) - \Delta h_E \tag{21}$$

Diffuser Performance

The diffuser static pressure rise coefficient was defined from the impeller exit to the collector and is given by:

$$C_p = \frac{P_{s3} - P_{s2}}{\overline{P}_{t2} - P_{s2}} \tag{22}$$

Diffuser losses were documented by the following:

$$\text{Diffuser loss (total-to-static)} = \frac{\overline{P}_{t2} - P_{s3}}{\overline{P}_{t2}} \tag{23}$$

$$\text{Diffuser loss (total-to-total)} = \frac{\overline{P}_{t2} - \overline{P}_{t3}}{\overline{P}_{t2}} \tag{24}$$

$$\text{Diffuser loss coefficient} = \frac{\overline{P}_{t2} - P_{s3}}{\overline{P}_{t2} - P_{s2}} \tag{25}$$

$$\text{Dump loss} = \frac{\overline{P}_{t3} - P_{s3}}{\overline{P}_{t3}} \tag{26}$$

where $\overline{P}_{t3}$ is the mass-average total pressure at the diffuser exit. The Mach No. profile at the diffuser exit was calculated, based on diffuser exit total pressure data and collector static pressure and assuming a γ of 1.4. Total pressure data from different pipes was first adjusted to match a single average value at the center of each pipe.

Diffuser throat blockage (B) was calculated assuming a throat Mach No. of 1.0 by

$$B = 1.0 - \text{flow factor}$$

where

$$\text{flow factor} = \frac{W_{net}\sqrt{T_3}}{\overline{P}_{t2} A^* 0.532} \tag{27}$$

VALIDATION OF TEST DATA

Estimates of the uncertainty of the data acquired from the shrouded impeller test rig are presented in Table 7. These estimates include both the uncertainty of the sensor and of the recording device. Uncertainty of air angle assumes no alignment error. Both bias (constant error) and precision errors (precision errors are two standard deviations from the mean) were used to determine the potential uncertainty, and are presented in Table 7. When multiple probes were available for redundant measurement, the precision error was calculated by statistically averaging individual measurements, as illustrated below.

$$u = \frac{e}{\sqrt{n}}$$

where

u = overall uncertainty of flow variable
e = uncertainty of individual sensor
n = number of sensors recording the same flow variable

Table 7 also includes the effect of the data uncertainty on the uncertainty of the overall efficiency performance calculation. This performance uncertainty estimate was calculated by differentiating the efficiency equation and inputting the uncertainty values in the resulting relationship. The uncertainty of the efficiency value was 0.53 percentage point, which was considered to be satisfactory.

An estimate of the uncertainty of the inlet orifice flow measurement is shown in Figure 16 as a function of inlet orifice flow rate. The uncertainties of the inducer bleed and shroud seal leakage flow measurements were each estimated to be approximately 4.0% of the respective measured flow rates.

At each steady-state point, approximately 20 scans of data recorded over a 2-sec interval were averaged. A typical printout from a near-stall, steady-state point at 101% design speed and 0-deg inlet guide vane setting is shown in Table 8. A 2-sec average value, the maximum and the minimum value recorded, and a three-sigma value (three standard deviations from the mean) are also listed for each instrumentation. These provide a measure of the actual scatter in the data due both to the uncertainty in measurement and to slight speed and flow variations that may have occurred while recording the steady state.

TABLE 7. ANALYSIS OF INSTRUMENTATION ACCURACY

Variable	Location (Station)	Type Instrument	Range	Number of Probes Averaged	Bias, ±	Precision, ±	Uncertainty, ±	Units
P_s	0	Transducer	0 to 15	3	0.04	0.01	0.05	psia
T	0	Resistance Thermometer	Ambient	5	0.27	0.07	0.34	°R
P_s	1 and 1.5	Pressure Scanner	0 to 15	4	0.05	0.02	0.07	psia
Air Angle	1.5 and 2	Potentiometer	0 to 160	1	0.4	1.2	1.6	deg
P_t	1.5	Transducer	0 to 25	1	0.40	0.30	0.43	psia
T	1.5	CA/TC	0 to 600	1	3.0	1.2	4.2	°R
P_t	2	Transducer	0 to 170	1	0.46	0.29	0.74	psia
P_s	2 and 3	Pressure Scanner	0 to 150	1	0.43	0.34	0.77	psia
T	3	CA/TC	0 to 1150	4	0.90	0.48	1.38	°R
Flow Rate	Inlet	Orifice	3.1	3 ΔP, 3 P_s, 5 T	0.024	0.037	0.059	lb/sec
Efficiency	0 to 3.5	-	75%	-	-	-	0.531	%

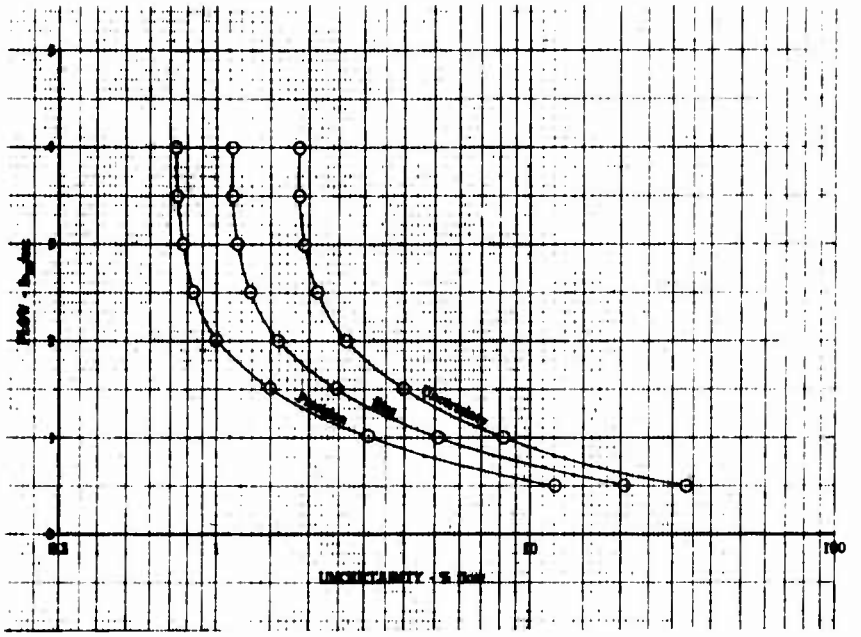

Figure 16. Inlet Orifice Flow Measurement Uncertainty.

Integrated flows calculated from inducer exit traverse data corresponded well with the inlet orifice flow, as shown in Figure 17. The impeller exit integrated flow correspondence was good for data obtained during runs 8.06 and 8.07 but shifted for data obtained during run 8.10, as shown in Figure 18. This shift was caused by an error in the flagging and alignment of the impeller exit cobra probe, which occurred while reinstalling the probe on the test stand prior to run 8.10. Prior to the calculation of component performance parameters and velocity triangles, the inducer exit and the impeller exit integrated flows were adjusted to match the measured flows at these stations, and thus satisfy continuity requirements. This was accomplished by adding a constant value to the measured air angle profiles to account for probe misalignment.

An externally aspirated collector total temperature probe was designed for use in the test program as described in the Instrumentation Section. During the test program, one of the aspirating probes was removed and replaced with one of the original Contract DAAJ02-70-C-0006 shielded total temperature probes for comparative purposes. As shown in Table 9, the two probes read within 3 deg (at 700°F) of each other at similar test point conditions and locations in the collector, which is good agreement for the two types of probes.

TABLE 8. TYPICAL PRINTOUT FOR A NEAR-STALL, STEADY-STATE POINT AT 101% DESIGN SPEED AND 0-DEG INLET GUIDE VANE SETTING

1/ TIME 1828 NOV 16, 1973 RIG NO. 3588 BUILD 08 RUN NO. 008.03 B-02

AVERAGES FOR THE TIME INTERVAL BEGINNING AT 2399.125

HEADER	UNITS	CHANNEL	AVERAGES	3xSIGMA	MAXIMUM	MINIMUM	SCANS USED	SCANS ELIMINATED
PERFA1	PSID	0	0.020	0.0	0.026	0.020	19	0
SHORT1	CNTS	1	0.0	0.0	0.0	0.0	19	0
PSC-01	PSIA	2	14.707	0.022	14.711	14.695	19	0
PSC-02	PSIA	3	14.677	0.029	14.702	14.670	19	0
PSC-03	PSIA	4	14.692	0.036	14.702	14.670	19	0
APSC--	PERF--	5	14.692	0.023	14.705	14.679	19	0
PSCD01	PSID	6	1.361	0.013	1.372	1.356	19	0
PSCD02	PSID	7	1.362	0.047	1.394	1.341	19	0
PSCD03	PSID	8	1.368	0.044	1.387	1.334	19	0
APSCD-	PERF--	9	1.364	0.026	1.378	1.346	19	0
TTP-01	DERT	10	544.140	0.162	544.196	544.091	19	0
TTP-02	DERT	11	543.405	0.145	543.499	543.288	19	0
TTP-03	DERT	12	543.719	0.100	543.814	543.708	19	0
TTP-04	DERT	13	543.630	0.148	543.710	543.602	19	0
TTP-05	DERT	14	543.554	0.192	543.720	543.510	19	0
ATTP--	PERF--	15	543.690	0.074	543.746	543.661	19	0
PTP-01	PSIA	16	13.539	0.0	13.539	13.539	19	0
PTP-02	PSIA	17	13.551	0.020	13.563	13.547	19	0
PTP-03	PSIA	18	13.545	0.018	13.558	13.542	19	0
APTP--	PERF--	19	13.545	0.011	13.553	13.543	19	0
TUTR-1	PERF--	20	541.418	0.195	541.561	541.374	19	0
SPEED1	RPM	21	67451.812	99.379	67542.875	67440.437	18	1
SPEED2	RPM	22	67545.312	444.516	67716.875	67207.750	19	0
RT1A01	USID	23	1.001	0.003	1.003	0.999	19	0
AA1AC1	USID	24	12.953	0.097	13.026	12.939	19	0
PT1A01	PERF--	25	20.659	0.129	20.708	20.556	19	0
TT1A01	PERF--	26	829.263	0.892	829.921	828.771	19	0
RT2-01	USID	27	0.505	0.003	0.505	0.503	19	0
AA2-01	PERF--	28	-70.411	0.060	-70.328	-70.416	19	0
PT2-01	PERF--	29	64.239	0.408	64.455	63.969	19	0
PREF--	PSIA	30	19.638	0.040	19.649	19.623	19	0
SVH--1	PERF--	31	48.000	0.0	48.000	48.000	19	0
SVP--1	PSID	32	0.007	0.039	0.022	-0.004	19	0
SVRP-1	PERF--	33	15.961	0.042	15.979	15.939	19	0
SVH--2	PERF--	34	48.000	0.0	48.000	48.000	19	0
SVP--2	PSIA	35	14.572	0.177	14.586	14.329	19	0

TABLE 8. CONTINUED

1/ TIME 1828 NOV 16, 1973 RIG NO. 3588 BUILD 08 RUN NO. 008.03 B-02

AVERAGES FOR THE TIME INTERVAL BEGINNING AT 2399.125

HEADER	UNITS	CHANNEL	AVERAGES	3xSIGMA	MAXIMUM	MINIMUM	SCANS USED	SCANS ELIMINATED
SVRP-2	PERF—	36	15.809	0.191	15.826	15.547	19	0
SVTT1	PERF—	37	551.847	0.652	552.355	551.706	19	0
SVTT2	PERF—	38	548.635	0.582	549.277	548.718	19	0
BLANK		39	100.008	0.0	100.000	100.000	19	0
APSBMO	PERF—	40	14.389	0.0	14.389	14.389	19	0
APS1S-	PERF—	41	12.460	0.0	12.460	12.460	19	0
APS1AS	PERF—	42	20.885	0.0	20.885	20.885	19	0
APSIR-	PERF—	43	50.764	0.0	50.764	50.764	19	0
APS2S4	PERF—	44	63.380	0.0	63.380	63.380	19	0
APS2H4	PERF—	45	59.779	0.0	59.779	59.779	19	0
APS38-	PERF—	46	129.011	0.0	129.011	129.011	19	0
PS3-06	PERF—	47	128.669	0.528	129.033	128.329	19	0
IGVACH	PERF—	48	86.500	0.221	86.665	86.468	19	0
BLANK		49	-9.737	2.974	-8.000	-11.000	19	0
TT3-01	PERF—	50	1146.165	1.543	1146.720	1145.101	19	0
TT3-02	PERF—	51	1144.764	1.371	1145.317	1144.111	19	0
TT3-03	PERF—	52	1154.713	1.515	1155.542	1153.747	19	0
TT3-04	PERF—	53	1145.734	2.198	1146.923	1144.087	19	0
ATT3—	PERF—	54	1147.844	1.310	1148.539	1147.077	19	0
TT3-05	PERF—	55	518.631	1.587	519.371	517.454	19	0
PT3-11	PERF—	56	134.463	0.416	134.743	134.232	19	0
PT3-12	PERF—	57	136.103	0.756	136.689	135.668	19	0
PT3-13	PERF—	58	130.887	0.611	131.220	130.577	19	0
BLANK	PERF—	59	1.000	0.0	1.000	1.000	19	0
TTBLAC	PERF—	60	851.607	1.463	852.311	850.714	19	0
TTBADR	DECA	61	663.322	1.415	663.950	662.481	19	0
PSBADR	PSIA	62	15.940	0.143	16.027	15.867	19	0
DELPBA	PSID	63	1.807	0.049	1.843	1.765	19	0
WACTBA	PERF—	64	0.027	0.000	0.028	0.027	19	0
TTSLAC	PERF—	65	1098.964	2.304	1099.967	1097.307	19	0
TTSLDR	DECA	66	686.071	1.372	686.843	685.737	19	0
PSSLDR	PSIA	67	19.965	0.189	20.109	19.896	19	0
DELPSL	PSID	68	8.228	0.081	8.279	8.200	19	0
WACTSL	PERF—	69	0.019	0.000	0.019	0.019	19	0
FCOXT1	PERF—	70	631.885	0.340	632.275	631.818	19	0
FBBTM1	PERF—	71	653.471	0.998	654.177	652.799	19	0

TABLE 8. CONTINUED

1/ TIME 1828 NOV 16, 1973 RIG NO. 3588 BUILD 08 RUN NO. 008.03 B-02

AVERAGES FOR THE TIME INTERVAL BEGINNING AT 2399.125

HEADER	UNITS	CHANNEL	AVERAGES	3xSIGMA	MAXIMUM	MINIMUM	SCANS USED	SCANS ELIMINATED
FRBTM2	DECA	72	549.811	1.014	550.257	548.953	19	0
RBTMP1	PERF—	73	607.486	1.223	608.011	606.548	19	0
WACT—	PERF—	74	2.738	0.024	2.751	2.723	19	0
TR——	PERF—	75	2.213	0.003	2.214	2.211	19	0
SHUM	PERF—	76	0.012	0.0	0.012	0.012	19	0
APTMA		77	122.526	5.601	126.000	120.000	19	0
WCORBA	PERF—	78	0.030	0.000	0.031	0.030	19	0
WCORSL	PERF—	79	0.021	0.000	0.021	0.021	19	0
WCOR—	PERF—	80	65933.250	228.119	66055.750	65759.625	19	0
WCOR—	PERF—	81	3.041	0.028	3.056	3.024	19	0
WCORNT	PERF—	82	2.990	0.028	3.005	2.973	19	0
PRST—	PERF—	83	8.757	0.036	8.781	8.733	19	0
TEFTTS	PERF—	84	0.692	0.002	0.694	0.691	19	0
TEFNLT	PERF—	85	0.684	0.002	0.685	0.682	19	0
PRS——	PERF—	86	8.780	0.0	8.780	8.780	19	0
EFFTTS	PERF—	87	0.693	0.001	0.694	0.693	19	0
EFFNET	PERF—	88	0.685	0.001	0.686	0.684	19	0
EFFHUM	PERF—	89	0.698	0.002	0.699	0.697	19	0
WCORR-	PERF—	90	65933.250	228.119	66055.750	65759.625	19	0
WCORR		91	88.684	4.904	90.000	86.000	19	0
PRTT—	PERF—	92	9.143	0.029	9.163	9.124	19	0
TEFTTT	PERF—	93	0.708	0.002	0.709	0.707	19	0
PRT——	PERF—	94	9.078	0.0	9.078	9.078	19	0
EFFTTT	PERF—	95	0.705	0.002	0.705	0.704	19	0
AMPRES		96	14.705	0.0	14.705	14.705	19	0
WCORR-	PERF—	97	3.041	0.028	3.056	3.024	19	0
APTMA-	PERF—	98	133.399	0.0	133.399	133.399	19	0
TDRY	PERF—	99	77.000	0.0	77.000	77.000	19	0

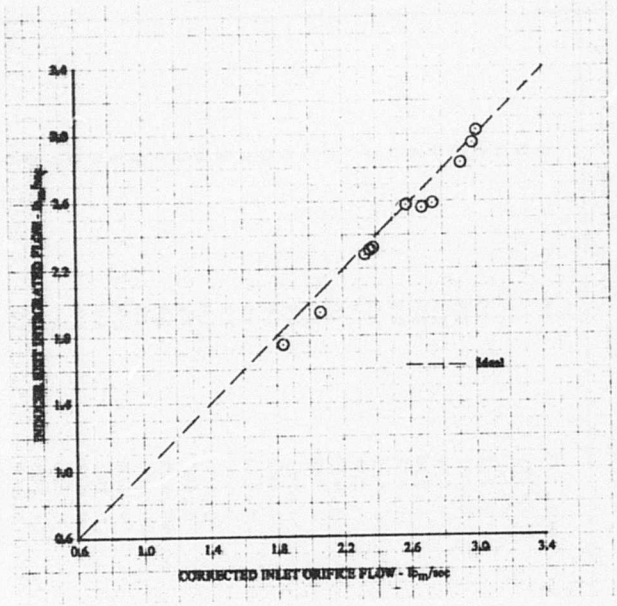

Figure 17. Inducer Exit Integrated Flow Correspondence.

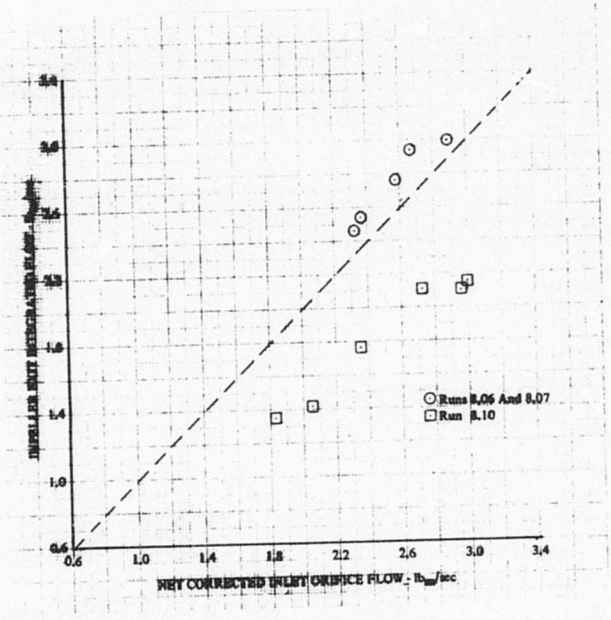

Figure 18. Impeller Exit Integrated Flow Correspondence.

TABLE 9. COLLECTOR TEMPERATURE PROBE COMPARISON

Test Point	10:1 Program Probe, °R	Aspirating Probe, °R	Δ, °R
101%, -4 deg IGV, No Bleed	1166.371	1164.056	-2.315
101%, -4 deg IGV, Max Bleed	1159.096	1155.948	-3.149
101%, 0 deg IGV, No Bleed	1157.331	1154.612	-2.719
101%, 0 deg IGV, Max Bleed	1152.494	1149.418	-3.076
96%, 0 deg IGV, No Bleed	1097.942	1094.902	-3.082
96%, 10 deg IGV, Max Bleed	1085.294	1082.079	-3.215
85%, 20 deg IGV, No Bleed	959.913	956.830	-3.083
80%, 20 deg IGV, No Bleed	914.801	911.897	-2.904

RESULTS AND DISCUSSION

OVERALL PERFORMANCE

The overall performance map for the Shrouded Impeller Test Program is presented in Figure 19 along with the peak efficiency and pressure ratio surge lines attained in Contract DAAJ02-70-C-0006, 10:1 Pressure Ratio Single-Stage Centrifugal Compressor Program (hereinafter referred to as "the 10:1 program"). A complete tabulation of overall performance data is listed in Table 10. Although the shrouded impeller performance is comparable to 10:1 performance levels up to approximately 70% speed, performance steadily deteriorates with increasing speed. A comparison of the maximum weight flows for the two programs, shown in Figure 20, exhibits the same trend. At 101% speed and 0-deg IGV, the shrouded impeller performance is down by 5.7 points in efficiency and 0.23 lb_m/sec in weight flow as compared with the unshrouded compressor performance at the same speed and IGV setting. This is an 8.2 percentage-point deficiency relative to the projected goals for the shrouded impeller, as outlined in Table 11. Of this 8.2 percentage-point deficiency, 3.7 result from high diffuser losses, with the remaining 4.5 attributed to the rotor. Causes of the larger than anticipated rotor and diffuser losses, which are discussed in detail later, include (1) operation of the rotor at higher than desired stalled incidence due to increased diffuser throat blockage, (2) separated flow at the impeller exit along the hub sidewall in the vaneless space, and (3) a spanwise flow incidence mismatch with the leading edge of the diffuser.

The effect of inducer bleed on overall performance is shown in Figure 21 for 96% speed, 10-deg IGV and 101% speed, 0-deg IGV settings. At the maximum bleed flow rate, the net efficiency at both speeds was increased by approximately 0.6 percentage points, along with slight increases in both pressure ratio and net weight flow. The associated inducer bleed and shroud seal leakage flow rates were presented in Figures 14 and 15, respectively, as a function of inlet orifice flow rate.

Overall performance data at 10, 20, and 30% design speeds are shown plotted on expanded scales in Figure 22. There was no discernible surge point at 10% speed as the impeller apparently produced pressure rise with the backpressuring valves completely closed with only leakage flow through the rig. Also, the pressure ratio produced at 10% speed was insufficient to balance the backface cavity, which resulted in thrust balance GN_2 flowing into the flow path at the impeller exit. This lowered the measured collector total temperature so that no accurate efficiency calculations could be made at this speed.

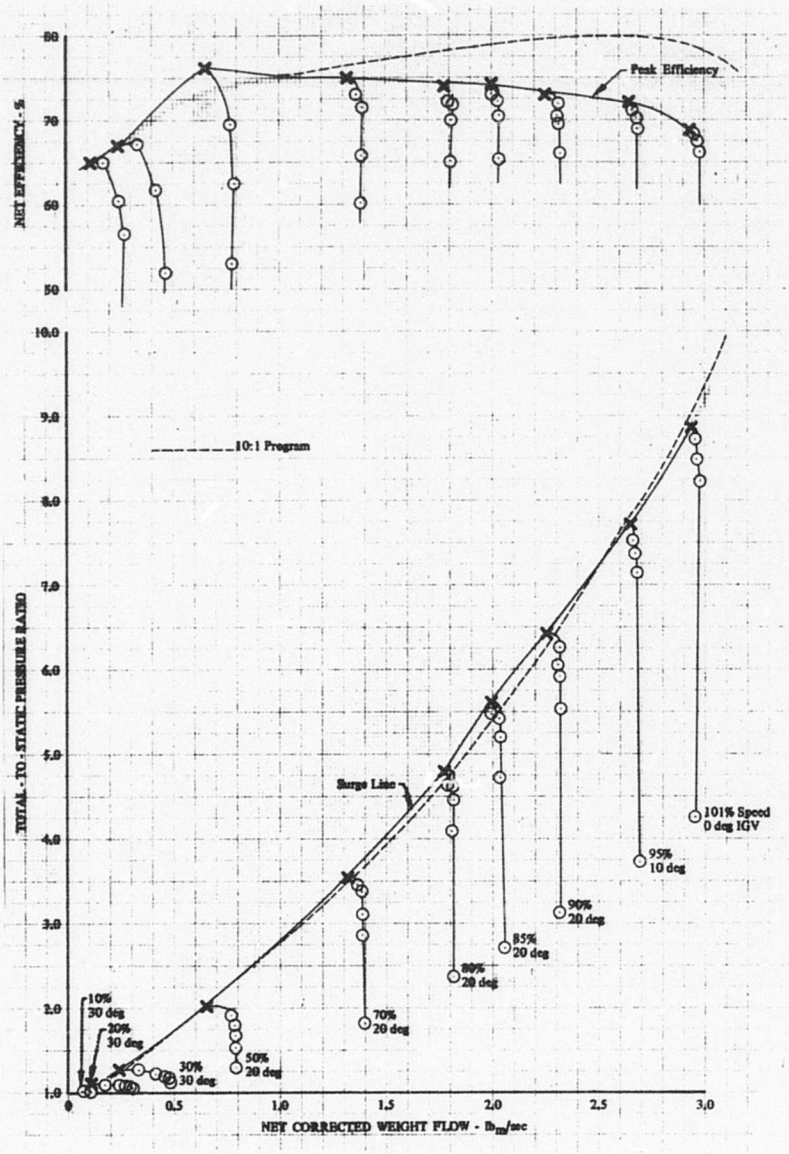

Figure 19. Shrouded Impeller Compressor Overall Performance (No Inducer Bleed Flow).

TABLE 10. OVERALL PERFORMANCE TABULATION

Speed, %	IGV Setting, deg	Net Weight Flow, lb_m/sec	Pressure Ratio	Net Efficiency
10	30	0.079	1.019	-
		0.110	1.010	-
		0.109	1.008	-
20	30	0.109	1.099	0.650
		0.175	1.096	0.650
		0.245	1.084	0.604
		0.272	1.074	0.566
		0.296	1.065	-
		0.303	1.052	-
30	30	0.242	1.276	0.670
		0.335	1.268	0.672
		0.419	1.236	0.618
		0.465	1.194	0.520
		0.481	1.156	-
		0.484	1.115	-
50	20	0.650	2.041	0.764
		0.769	1.892	0.682
		0.785	1.809	0.627
		0.782	1.656	0.523
		0.787	1.534	0.438
		0.793	1.278	-
70	20	1.320	3.563	0.750
		1.361	3.469	0.733
		1.387	3.338	0.705
		1.387	3.121	0.659
		1.388	2.855	0.598
		1.395	1.828	0.330
80	20	1.770	4.809	0.741
		1.796	4.664	0.725
		1.809	4.609	0.716
		1.810	4.467	0.700
		1.805	4.083	0.650
		1.814	2.378	0.370
85	20	1.992	5.631	0.743
		1.994	5.470	0.730
		2.032	5.376	0.722
		2.036	5.210	0.706
		2.034	4.723	0.654
		2.054	2.707	0.388

TABLE 10. CONTINUED

Speed, %	IGV Setting, deg	Net Weight Flow, lb_m/sec	Pressure Ratio	Net Efficiency
90	20	2.253	6.433	0.731
		2.317	6.244	0.719
		2.309	6.079	0.708
		2.317	5.931	0.695
		2.321	5.535	0.660
		2.311	3.104	0.401
	10	2.290	6.602	0.731
		2.341	6.321	0.712
		2.338	6.195	0.704
		2.344	6.029	0.690
		2.334	5.536	0.649
		2.357	3.173	0.402
	0	2.335	6.622	0.716
		2.353	6.365	0.700
		2.357	6.247	0.690
		2.365	6.049	0.675
		2.362	5.440	0.623
		2.368	3.202	0.398
96	20	2.532	7.444	0.722
		2.547	7.202	0.710
		2.564	7.045	0.701
		2.562	6.844	0.688
		2.567	6.547	0.667
		2.560	3.541	0.408
	10	2.649	7.721	0.721
		2.664	7.562	0.715
		2.674	7.399	0.705
		2.684	7.169	0.690
		2.658	6.521	0.645
		2.693	3.722	0.417
	0	2.681	7.906	0.713
		2.698	7.752	0.706
		2.691	7.539	0.693
		2.689	7.296	0.678
		2.707	6.539	0.630
		2.736	3.806	0.415
101	10	2.890	8.619	0.698
		2.894	8.531	0.696
		2.912	8.331	0.687
		2.911	8.126	0.678
		2.888	7.357	0.635
		2.926	4.156	0.415

TABLE 10. CONTINUED

Speed, %	IGV Setting, deg	Net Weight Flow, lb_m/sec	Pressure Ratio	Net Efficiency
101	0	2.935	8.881	0.689
		2.956	8.786	0.687
		2.963	8.515	0.678
		2.981	8.251	0.662
		2.955	7.795	0.642
		2.977	4.266	0.413
	-4	2.991	9.058	0.690
		2.980	8.843	0.683
		2.993	8.675	0.676
		2.988	8.302	0.660
		2.977	7.778	0.635
		3.011	4.313	0.416
96 (With Inducer Bleed)	20	2.554	7.498	0.729
		2.568	7.318	0.720
		2.585	7.215	0.715
		2.590	7.016	0.702
		2.605	6.560	0.667
		2.591	3.572	0.414
	10	2.674	7.852	0.727
		2 705	7.647	0.719
		2.721	7.465	0.709
		2.725	7.243	0.695
		2.686	6.616	0.655
		2.715	3.777	0.423
	0	2.668	7.956	0.711
		2.702	7.877	0.706
		2.739	6.647	0.639
		2.730	3.812	0.416
101 (With Inducer Bleed)	10	2.912	8.719	0.706
		2.917	8.637	0.701
		2.932	8.383	0.692
		2.932	8.223	0.686
		2.922	7.240	0.632
		2.940	4.149	0.417
	0	2.958	8.989	0.695
		2.990	8.780	0.685
		3.000	8.704	0.689
		3.009	8.366	0.670
		3.001	7.715	0.632
		3.002	4.281	0.413

TABLE 10. CONTINUED				
Speed, %	IGV Setting, deg	Net Weight Flow, lb_m/sec	Pressure Ratio	Net Efficiency
101	-4	2.987	9.133	0.694
(With Inducer Bleed)		3.003	8.982	0.689
		3.004	8.805	0.685
		3.024	8.436	0.664
		3.000	7.778	0.640
		3.023	4.324	0.413

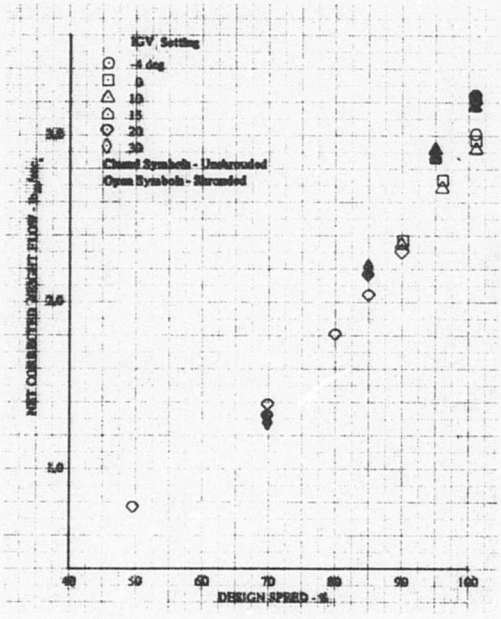

Figure 20. Shrouded and Unshrouded Impeller Maximum Weight Flow Comparison.

TABLE 11. COMPRESSOR EFFICIENCY SUMMARY (100% SPEED, 0-DEG IGV)	
Projected 10:1 Performance With Good Diffuser	75.2%
Net Change Shroud Addition	+3.0%
Net Change Rotating Vaneless Space and Diffuser Vaneless Space Addition	-0.5%
Projected Performance for Shrouded Impeller With Build 6 Rotor/Diffuser Match	77.7%
Demonstrated Shrouded Impeller	69.5%
Net Efficiency Change	-8.2%

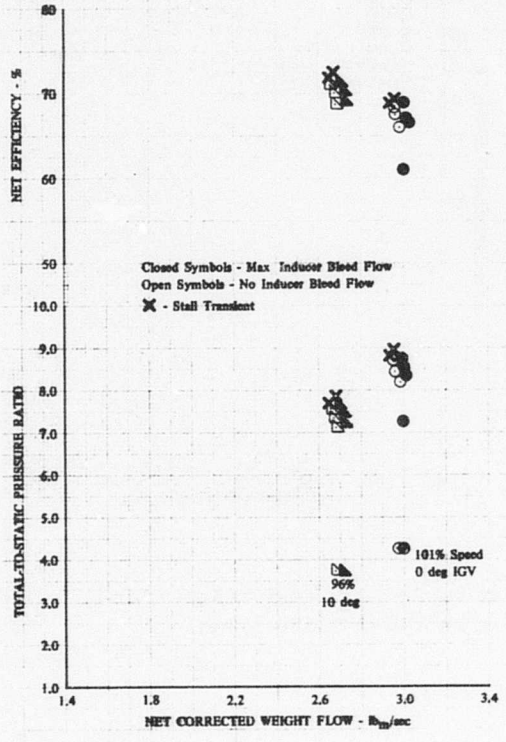

Figure 21. Effect of Inducer Bleed on Compressor Overall Performance.

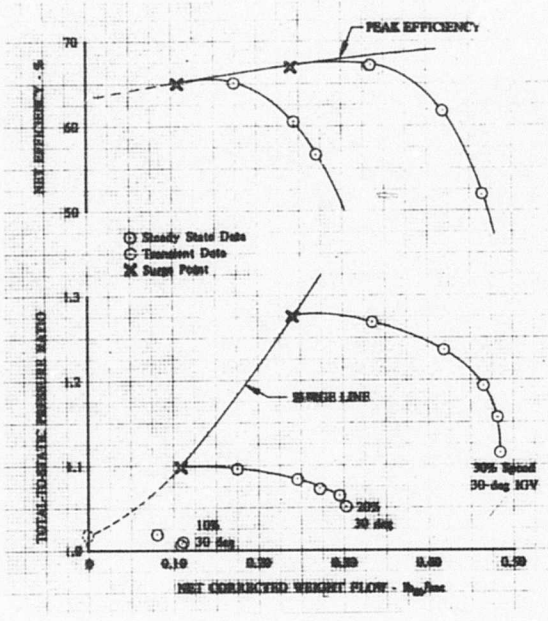

Figure 22. Low-Speed Overall Performance.

INDUCER PERFORMANCE

Inducer performance for the shrouded impeller test differs significantly from the performance demonstrated in the 10:1 program, as shown in Figure 23. Inducer efficiency is poorer by approximately 1.0% at 100% speed, and substantially worse at 96% speed, though the inducer is producing considerably greater pressure ratio at these speeds. Part of the loss in inducer performance can be attributed to the reduced flow rate and resultant more stalled incidence in the shrouded impeller test. Opening the inducer bleed increased flow and decreased incidence values, resulting in up to 2% inducer efficiency gains for nearly all points tested, as shown in Figure 24. Inducer incidence and inlet relative Mach No. (both with and without inducer bleed flow), along with the 10:1 program values, are shown in Figures 25 and 26 for 96% speed, 10-deg IGV and 101% speed, 0-deg IGV, respectively.

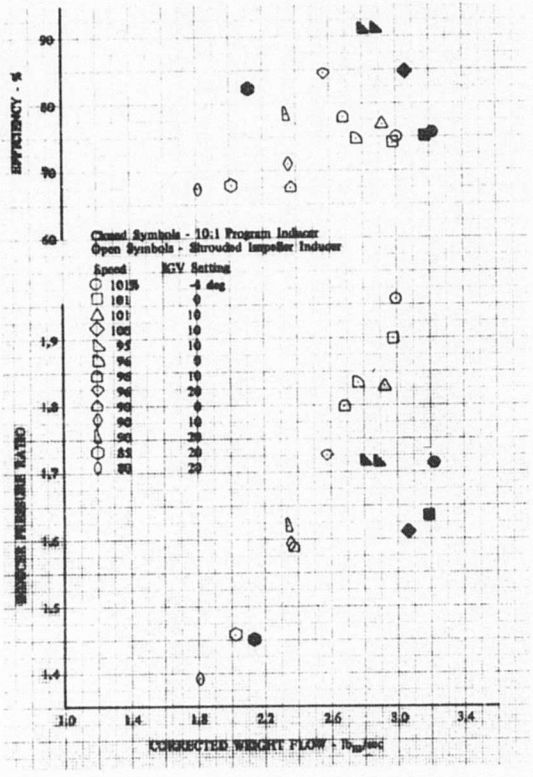

Figure 23. Comparison of Inducer Performance for Shrouded Impeller and 10:1 Program Inducers.

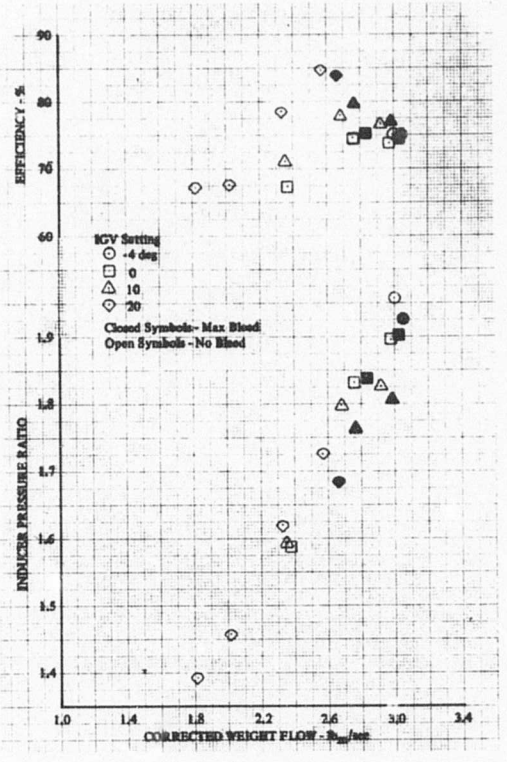

Figure 24. Effect of Inducer Bleed on Inducer Performance.

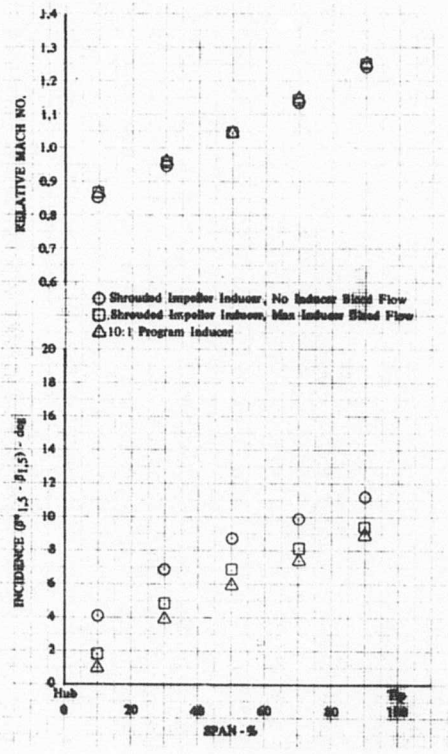

Figure 25. Shrouded Impeller Inducer Inlet Conditions (96% Speed, 10-deg IGV).

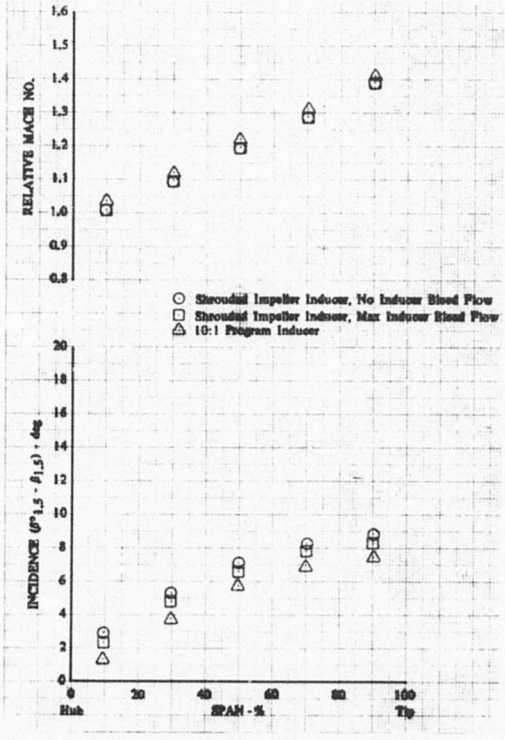

Figure 26. Comparison of Inducer Inlet Conditions for Shrouded Impeller and 10:1 Program Inducers (101% Speed, 0-deg IGV).

Part of the performance loss can also be attributed to heat transfer from the shroud cases into the flowpath, which was not accounted for in the data reduction program. In the absence of any temperature traversing behind the inlet guide vanes, the flowpath total temperature at this station was assumed to be ambient. However, the shroud case temperature at the inducer exit traversing plane was approximately 70 deg hotter at 101% speed in the shrouded impeller test than it was during Build 6 testing of the 10:1 program, as shown in Figure 27. Heat transfer into the flowpath upstream of the inducer was not measured, which results in an apparent higher temperature ratio across the inducer.

The compressor rig incorporated a "thermal dam" between the inducer shroud flange and the impeller housing flange, as shown in Figure 27, which allowed cooling with nitrogen for reducing heat transfer to cases upstream of the diffuser. This cooling simulated a thermal environment equivalent to that of a gas generator with thin-walled cases. In the typical example represented in Figure 27, when the coolant to the thermal dam was turned on, the three case temperatures measured decreased by an average of 58° F, and overall efficiency increased by 0.5 percentage points. A similar benefit was noted in the 10:1 program.

A comparison of the inducer exit relative velocity profiles is shown in Figure 28 for 101% speed and 0-deg IGV. As shown, not a great deal of difference exists in the velocity profiles; in fact, the profile for the shrouded impeller inducer appears to slightly improve in the tip region over the unshrouded impeller inducer. This can probably be attributed to the tighter inducer tip clearances run for the shrouded impeller tests. Total pressure, air angle, and total temperature profiles across the span at the inducer exit are presented in Figures 29 and 30 for 95% speed, 10-deg IGV and 101% speed, 0-deg IGV, respectively. The rapid increase in total temperature towards the shroud wall should be noted. Complete velocity triangle data are given in the traverse data reduction printouts in Table 12 for these two speedlines.

IMPELLER PERFORMANCE

Combined inducer-impeller (rotor) performance is presented along with the Build 6 rotor performance in Figure 31. At 85% speed, 20-deg IGV, where the weight flows were approximately identical, the shrouded impeller net rotor efficiency is 3.0 percentage points higher than the Build 6 rotor efficiency. As speed is increased, however, both flow rate and rotor efficiency fall steadily below Build 6 values. Shrouded impeller-only performance is compared to the Build 6 unshrouded impeller performance in Figure 32. At 85% speed the shrouded impeller shows approximately 8 percentage points better efficiency, while producing the same pressure ratio at the same flow as the unshrouded impeller. Again, as speed increases, performance deteriorates steadily.

Two possible causes for the drop in rotor performance at high speeds are (1) operation of the inducer at stalled incidence, as discussed in the inducer performance section, and (2) separation of the impeller exit flow along the hub wall in the vaneless space.

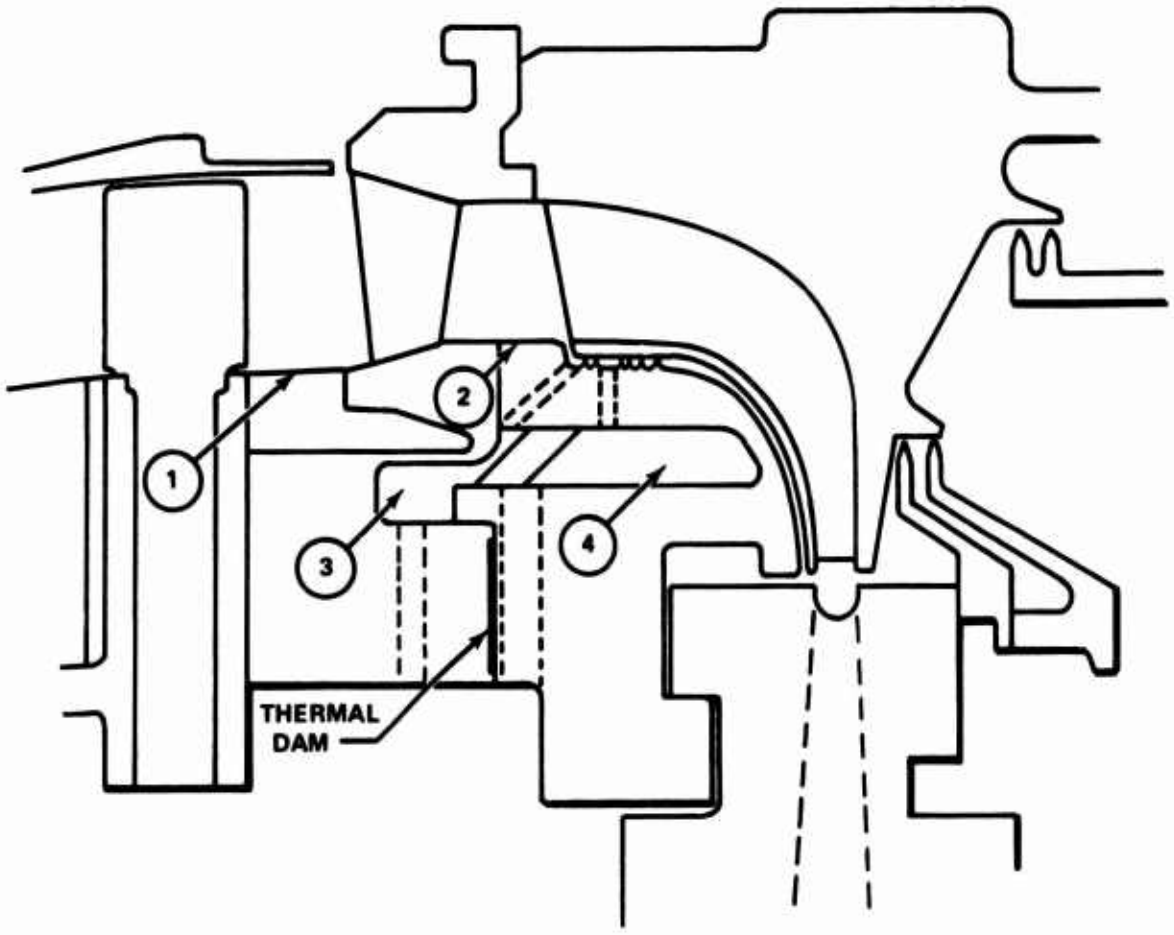

CONDITION	CASE TEMPERATURE, °R			
	1	2	3	4
10:1 TEST - THERMAL DAM OFF	625.6	758.7	—	—
SHROUDED - THERMAL DAM ON	—	785.9	766.2	1053.9
SHROUDED - THERMAL DAM OFF	—	829.3	851.6	1098.9

Figure 27. Compressor Rig Case Temperature Comparison (101% Speed, 0-deg IGV).

Figure 33 shows rotor adiabatic efficiency as a function of inlet tip relative flow angle for various rotor speeds. As is shown, a 2-3% rotor efficiency improvement could be realized by operation of the shrouded impeller rotor at the same inducer tip incidence as the unshrouded impeller. The increase in rotor net

efficiency gained by approximately 1.5% inducer bleed flow is presented in Figure 34. In addition to reducing incidence values, the bleed has an added effect on rotor performance by reducing the hot shroud boundary layer at the impeller inlet.

Separation of the impeller exit flow is indicated in the meridional velocity profiles in Figures 35 and 36 for 95% speed, 10-deg IGV and 101% speed, 0-deg IGV, respectively. The apparent flow separation occurs along the hub wall and comprises approximately 10-15% of the span. Also shown on each of these figures is the meridional velocity profile for the unshrouded impeller operating at comparable speed and IGV settings. While the unshrouded impeller appears to have the flow concentrated along the hub wall (with a large meridional boundary layer defect along the shroud), the shrouded impeller is just the opposite. This implies that addition of the shroud makes a pronounced improvement in the shroud wall boundary layer. For this particular impeller, however, the hub boundary layer deteriorates as much as the shroud boundary layer improves. A typical total pressure and air angle profile comparison at the impeller exit for 101% speed, 0-deg IGV is shown in Figure 37. Reduced traverse data defining the impeller exit conditions for 95% speed, 10-deg IGV and 101% speed, 0-deg IGV are presented in Table 13.

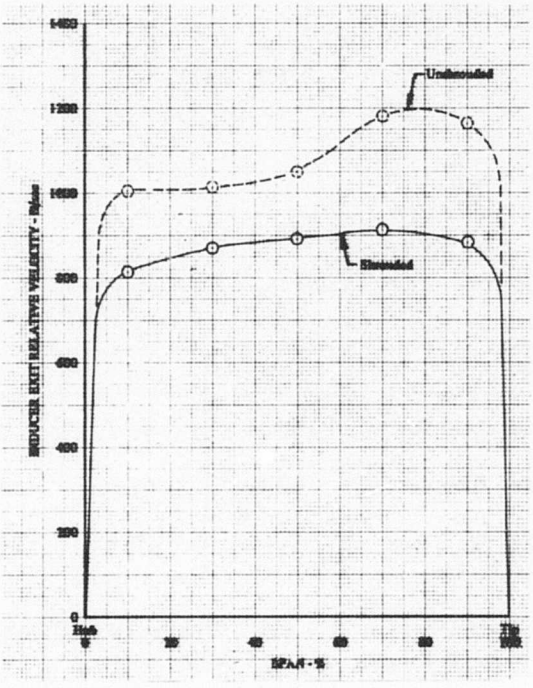

Figure 28. Comparison of Inducer Exit or Impeller Inlet Relative Velocity Profiles for Shrouded and Unshrouded Impellers (101% Speed, 0-deg IGV).

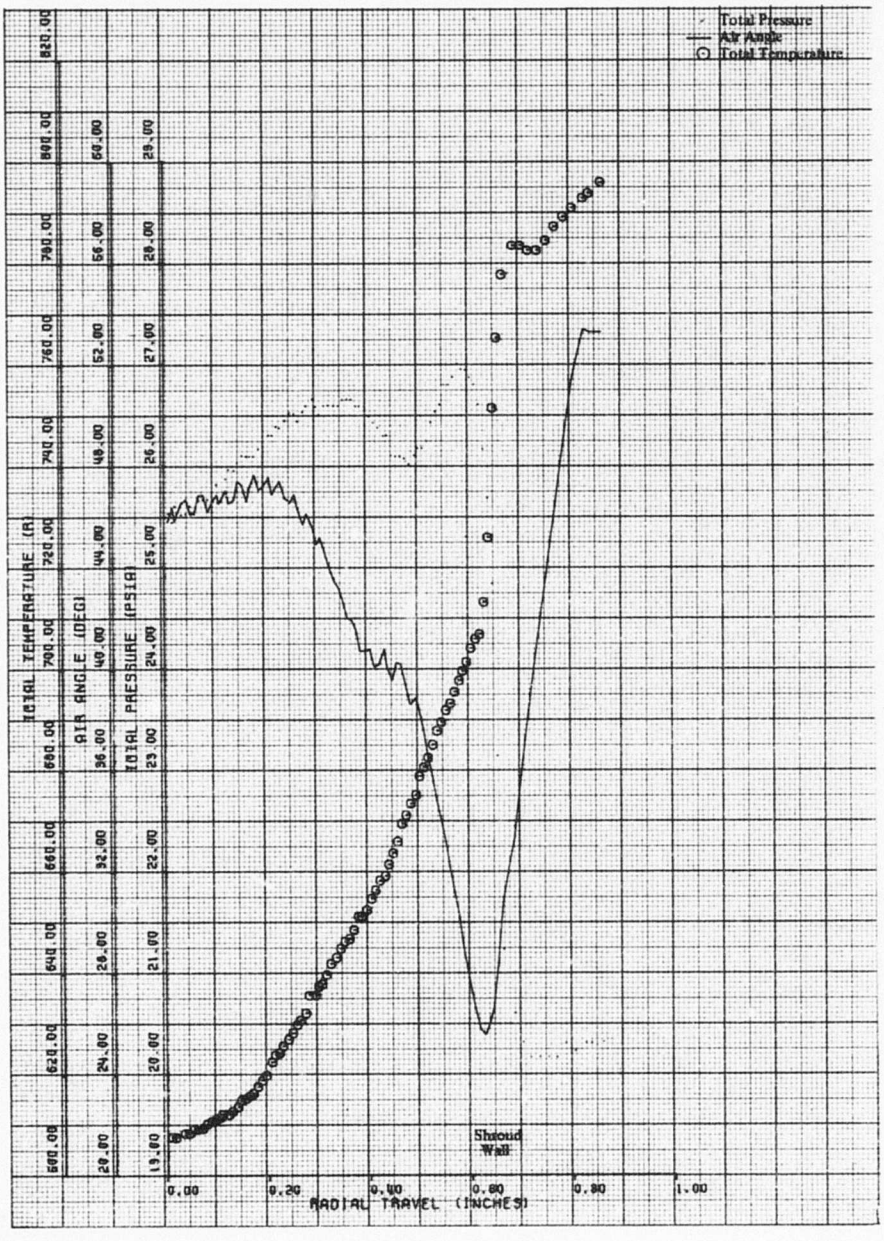

Figure 29. Inducer Exit Traverse (95% Speed, 10-deg IGV, No Bleed).

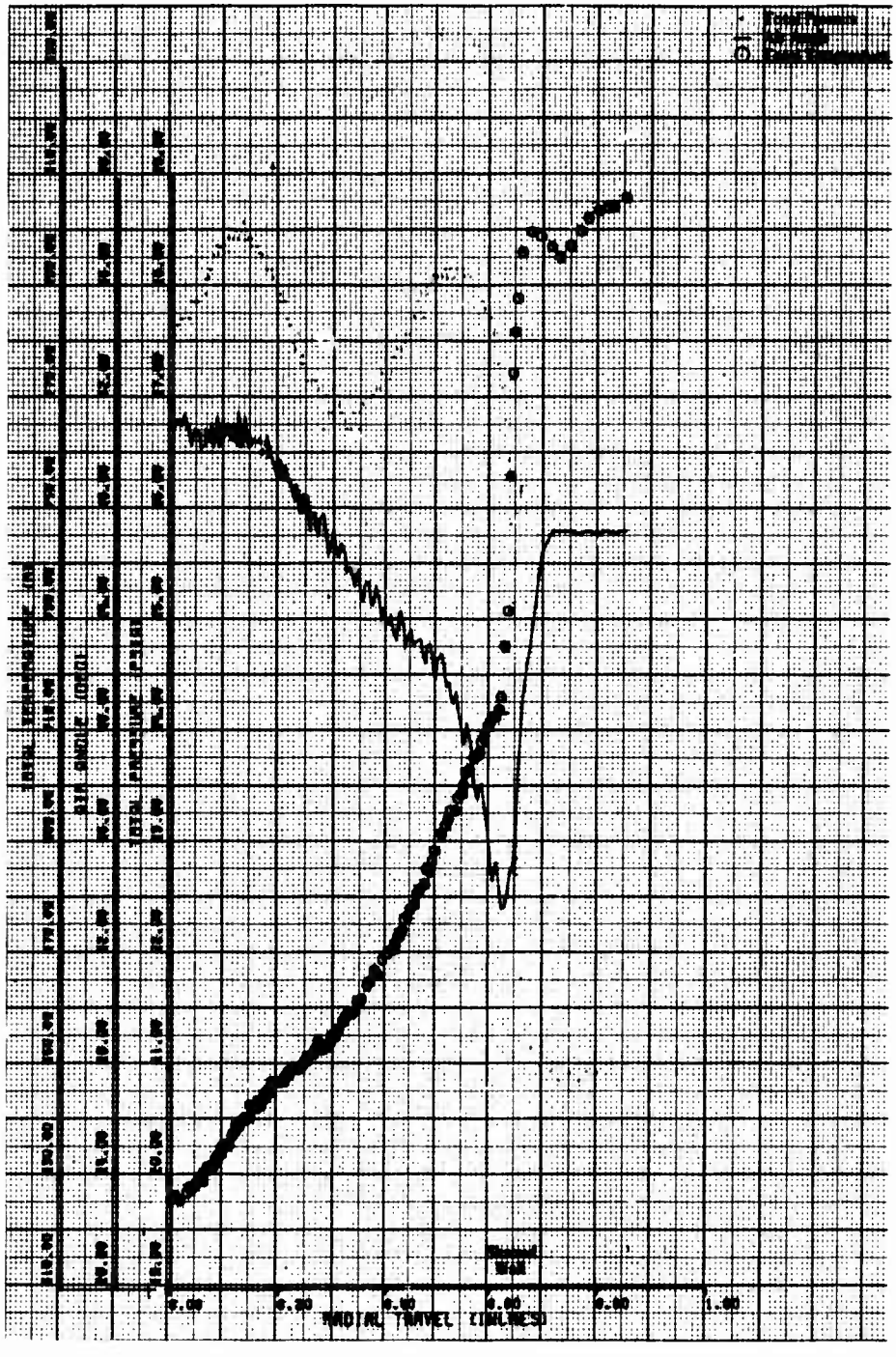

Figure 30. Inducer Exit Traverse (101% Speed, 0-deg IGV, No Bleed).

TABLE 12. INDUCER EXIT TRAVERSE DATA REDUCTION PRINTOUTS

10/1 SHROUDED IMPELLER BUILD 8
95 PCT SPEED 10 DEG IGV
NO BLEED FLOW

FLOW RATE = 2.681 SPEED = 62590.6

BLEED FLOW = 0.000 SEAL LEAKAGE FLOW = 0.019

* * * INDUCER EXIT * * * INITIAL INTEGRATED FLOW 2.565

MASS AVERAGE TOTAL PRESSURE 26.263
MASS AVERAGE TOTAL TEMPERATURE 640.812
INDUCER PRESSURE RATIO 1.787
INDUCER TEMPERATURE RATIO 1.235
INDUCER EFFICIENCY 0.765

INDUCER EXIT VELOCITY TRIANGLES

MO	VO	ALPHA	VM	VU	U	WU	B	WO	MREL	I	VO/VOMAX
KAA= 8		TOLERANCE=	-0.0076831								
10	0.563	659.355	48.700	495.353	435.172	990.297	555.125	41.743	744.002	0.635	11.956	0.846
30	0.579	681.088	49.496	517.872	442.368	1068.577	626.208	39.590	812.606	0.691	9.809	0.874
50	0.617	732.395	47.015	535.772	499.350	1146.856	647.506	39.605	840.426	0.709	5.424	0.939
70	0.589	714.561	42.333	481.213	528.234	1225.135	696.901	34.625	846.899	0.698	5.574	0.916
90	0.628	779.265	31.068	402.147	667.481	1303.414	635.933	32.308	752.418	0.607	3.341	1.000

10/1 SHROUDED IMPELLER BUILD 8
101 PCT SPEED 0 DEG IGV
NO BLEED FLOW

FLOW RATE = 2.979 SPEED = 65798.4

BLEED FLOW = 0.000 SEAL LEAKAGE FLOW = 0.021

* * * INDUCER EXIT * * * INITIAL INTEGRATED FLOW 2.949

MASS AVERAGE TOTAL PRESSURE 27.705
MASS AVERAGE TOTAL TEMPERATURE 660.649
INDUCER PRESSURE RATIO 1.885
INDUCER TEMPERATURE RATIO 1.273
INDUCER EFFICIENCY 0.723

INDUCER EXIT VELOCITY TRIANGLES

MO	VO	ALPHA	VM	VU	U	WU	B	WO	MREL	I	VO/VOMAX
KAA= 9		TOLERANCE=	-0.0097525								
10	0.624	738.043	51.261	575.676	461.848	1041.051	579.202	44.825	816.627	0.691	8.874	0.939
30	0.642	763.573	50.831	591.989	482.279	1123.342	641.062	42.720	872.585	0.734	6.679	0.972
50	0.589	712.983	47.298	523.969	483.529	1205.633	722.103	35.965	892.176	0.737	9.064	0.907
70	0.613	752.797	44.067	523.573	540.901	1287.924	747.022	35.025	912.234	0.743	5.174	0.958
90	0.628	785.939	37.260	475.478	625.043	1370.215	745.172	32.541	883.946	0.707	3.108	1.000

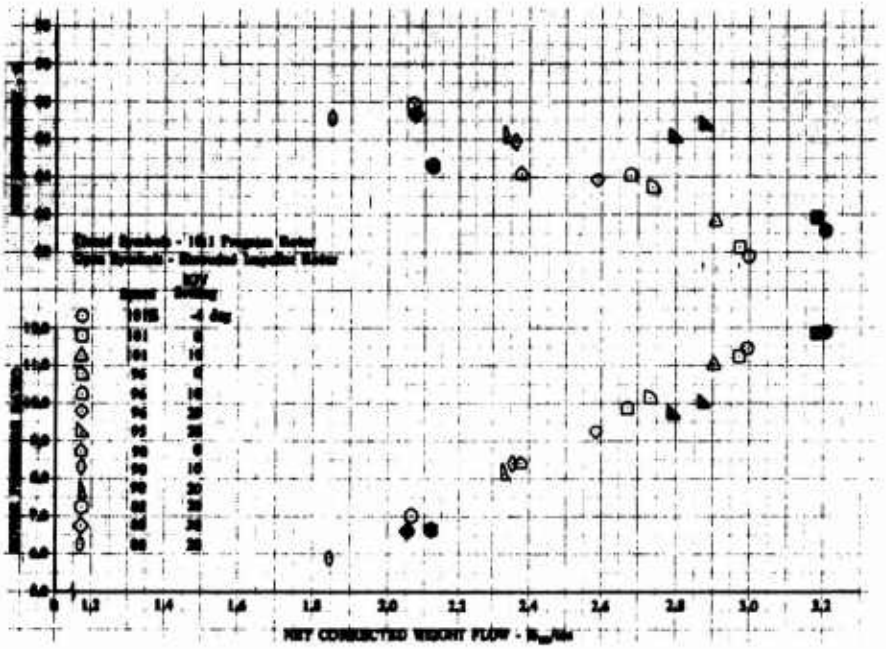

Figure 31. Comparison of Rotor Performance for Shrouded Impeller and 10:1 Program Rotors.

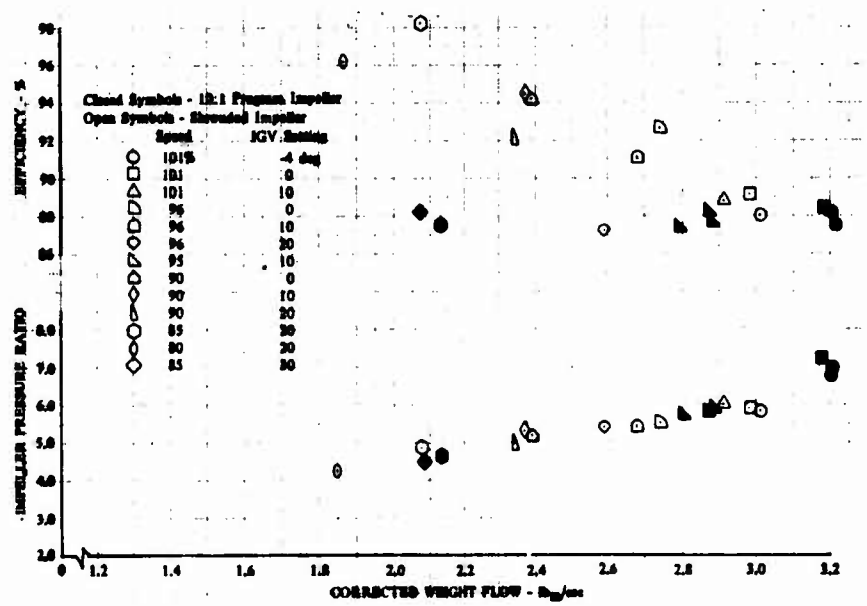

Figure 32. Comparison of Impeller Performance for Shrouded and 10:1 Program Impellers.

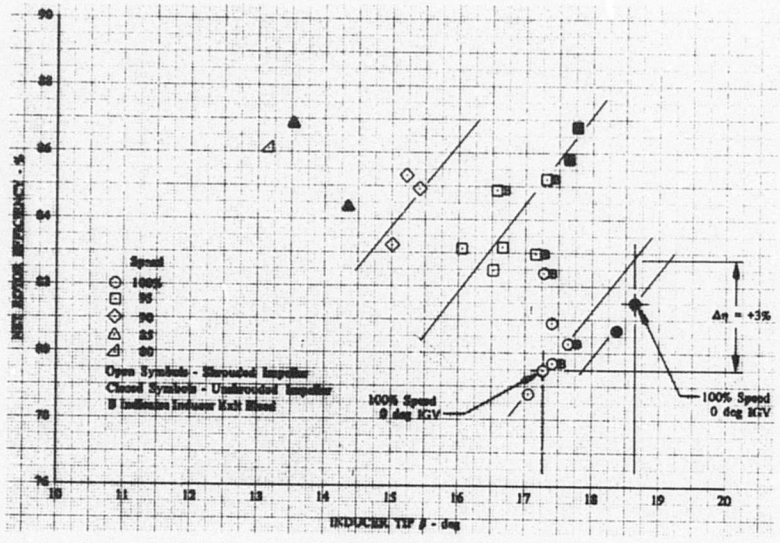

Figure 33. Effect of Inducer Inlet Tip Relative Flow Angle on Rotor Efficiency.

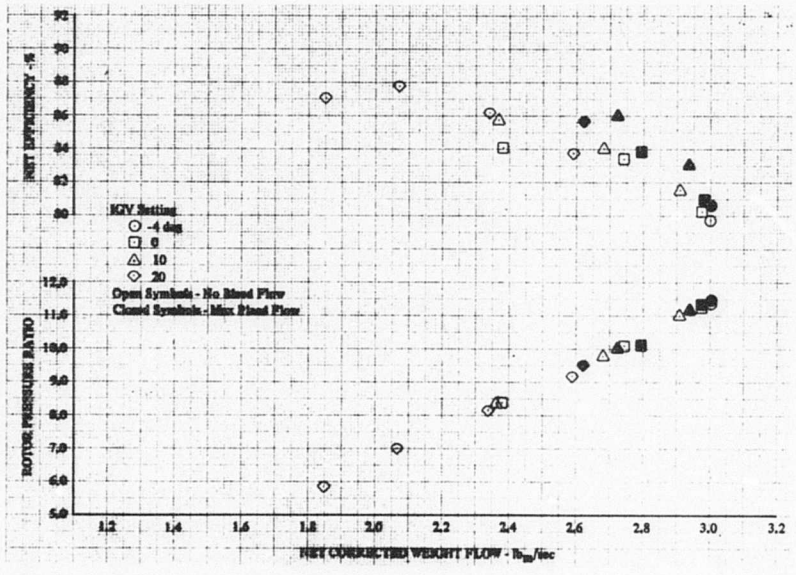

Figure 34. Effect of Inducer Bleed on Shrouded Impeller Rotor Performance.

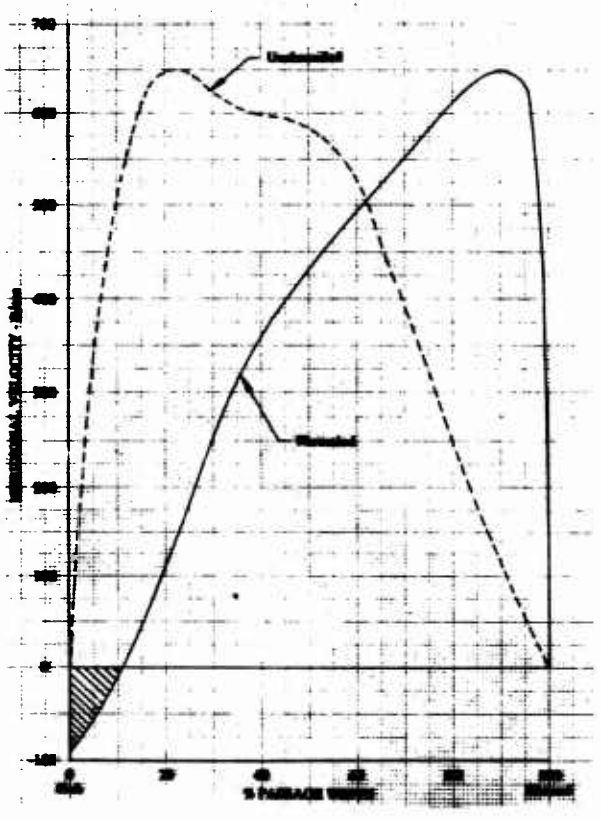

Figure 35. Comparison of Traverse Plane Meridional Velocity Profiles for Shrouded and Unshrouded Impellers (95% Speed, 10-deg IGV).

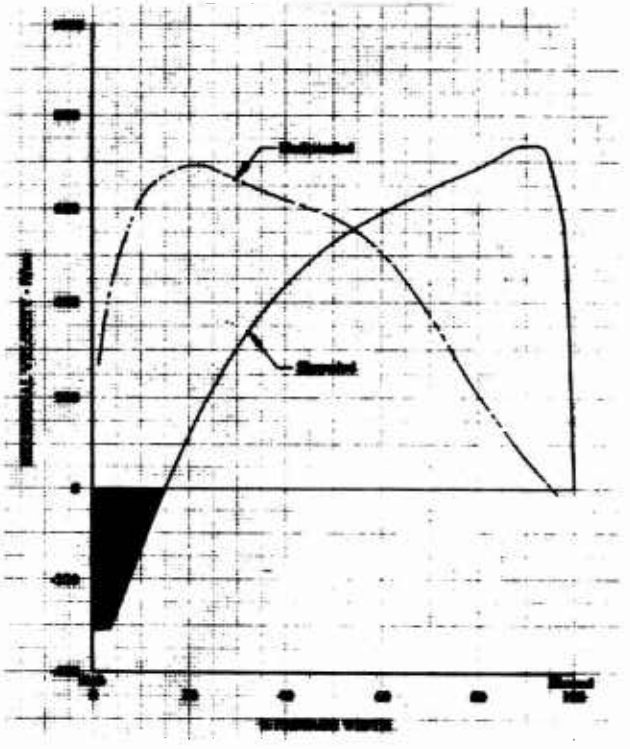

Figure 36. Comparison of Traverse Plane Meridional Velocity Profiles for Shrouded and Unshrouded Impellers (101% Speed, 0-deg IGV).

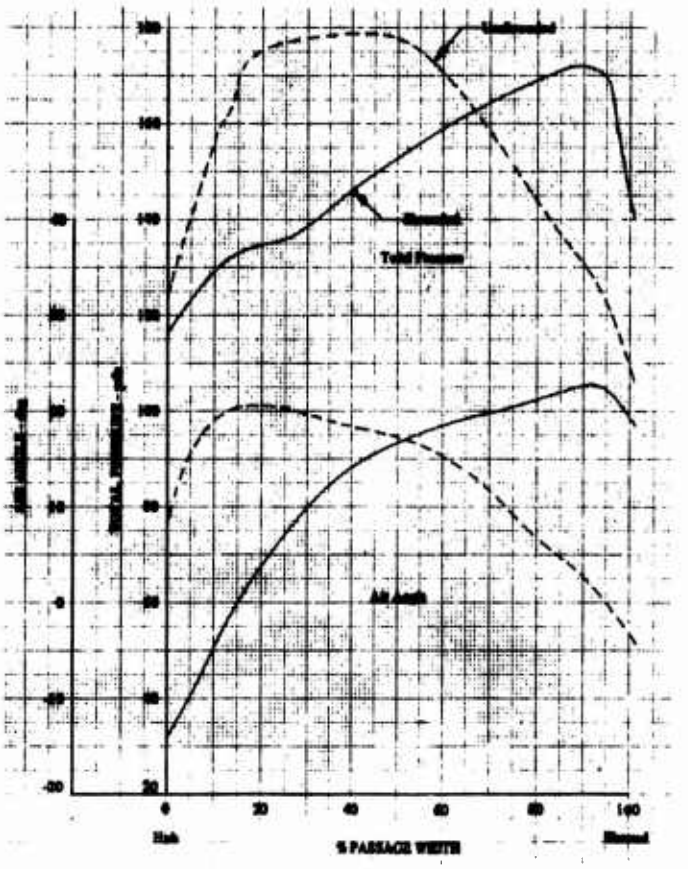

Figure 37. Comparison of Shrouded and Unshrouded Impeller Exit Traverse Data (101% Speed, 0-deg IGV).

A review of the design impeller exit velocity profiles for both the shrouded and unshrouded impellers, as shown in Figure 38, fails to reflect the drastic flow shifts shown in Figures 35, 36, and 37. Also in line with this, as illustrated in Figure 39, addition of the shroud and changing of the blade thickness and thickness distributions throughout the impeller did not substantially change the predicted hub boundary layer shape factor.

Static pressures at the impeller exit are compared to the 10:1 program values for similar test conditions in Table 14. The lower rim static pressures observed for the shrouded impeller test, which are measured in the pressure communicating groove, are probably influenced by the seal leakage flow. Good agreement exists between the impeller backface cavity static pressures in spite of the lower overall flow rates for the shrouded impeller test at 101% speed.

TABLE 13. IMPELLER EXIT TRAVERSE DATA REDUCTION PRINTOUTS

10/1 SHROUDED IMPELLER BUILD 8
95 PCT SPEED 10 DEG IGV
NO BLEED FLOW

FLOW RATE = 2.681 SPEED = 62590.6

BLEED FLOW = 0.000 SEAL LEAKAGE FLOW = 0.019

* * * IMPELLER EXIT * * * INITIAL INTEGRATED FLOW 2.990

PCENT SPAN	R	MO	VO	VO/VMAX	ALP	VM	VM/VMMAX	VU	U	WU	B	MO
0.0298	0.0070	0.8900	1328.87	0.7509	-2.969	-68.84	-0.1065	1327.09	1940.58	613.49	65.189	-75.84
0.0639	0.0149	0.9871	1452.06	0.8205	-1.719	-43.57	-0.0674	1451.41	1940.58	489.17	71.374	-45.98
0.1066	0.0249	1.0453	1523.59	0.8610	-0.219	-5.84	-0.0090	1523.58	1940.58	416.99	74.693	-6.05
0.1705	0.0399	1.0652	1546.71	0.8740	2.530	68.28	0.1056	1545.20	1940.58	395.37	75.647	70.48
0.2558	0.0599	1.0921	1578.72	0.8921	6.780	186.38	0.2884	1567.68	1940.58	372.89	76.620	191.58
0.3411	0.0799	1.1250	1616.31	0.9134	10.530	295.38	0.4571	1589.09	1940.58	351.48	77.527	302.52
0.4264	0.0999	1.1636	1660.51	0.9383	13.030	374.38	0.5794	1617.76	1940.58	322.82	78.715	381.77
0.5117	0.1199	1.1964	1696.70	0.9588	14.780	432.85	0.6698	1640.56	1940.58	300.01	79.636	440.02
0.5970	0.1399	1.2234	1726.32	0.9755	16.280	483.95	0.7489	1657.10	1940.58	283.48	80.292	490.98
0.6823	0.1599	1.2421	1746.39	0.9869	17.780	533.29	0.8253	1662.97	1940.58	277.60	80.522	540.67
0.7675	0.1799	1.2562	1761.30	0.9953	19.530	588.81	0.9112	1659.96	1940.58	280.61	80.404	597.16
0.8315	0.1949	1.2644	1769.53	1.0000	20.780	627.80	0.9715	1654.41	1940.58	286.16	80.166	637.12
0.8742	0.2049	1.2632	1767.89	0.9990	21.280	641.62	0.9929	1647.35	1940.58	293.23	79.907	651.70
0.9168	0.2150	1.2386	1741.45	0.9841	21.780	646.16	1.0000	1617.13	1940.58	323.44	78.689	658.95
0.9594	0.2249	1.1414	1633.06	0.9228	22.030	612.55	0.9479	1513.83	1940.58	426.74	74.256	636.43

MASS AVE TOT. PRESS. 142.657
MASS AVE TOT. TEMP. 1074.399

IMP.PRESS.RATIO 5.431 TEMP.RATIO 1.676 EFF 0.909
IMP..IND.PRESS.RATIO 9.767 TEMP.RATIO 2.071 EFF 0.841 NET EFF 0.841

TABLE 13. CONTINUED

10/1 SHROUDED IMPELLER BUILD 8
101 PCT SPEED 0 DEG IGV
NO BLEED FLOW

FLOW RATE = 2.979 SPEED = 65798.4

BLEED FLOW = 0.000 SEAL LEAKAGE FLOW = 0.021

* * * IMPELLER EXIT * * * INITIAL INTEGRATED FLOW 2.122

PCENT SPAN	R	MO	VO	VO/VMAX	ALP	VM	VM/VMMAX	VU	U	WU	B	WO
0.0426	0.0100	1.0640	1596.62	0.8434	-10.305	-285.63	-0.3902	1570.87	2040.03	469.16	73.370	-298.09
0.0852	0.0199	1.1003	1640.63	0.8667	-6.055	-173.07	-0.2364	1631.48	2040.03	408.55	75.941	-178.41
0.1279	0.0300	1.1226	1667.43	0.8808	-2.055	-59.80	-0.0817	1666.35	2040.03	373.67	77.360	-61.29
0.1705	0.0399	1.1355	1682.81	0.8889	1.694	49.76	0.0679	1682.07	2040.03	357.95	77.986	50.87
0.2132	0.0499	1.1414	1689.42	0.8924	4.944	145.61	0.1989	1683.14	2040.03	356.89	78.028	148.84
0.2558	0.0600	1.1449	1693.59	0.8946	7.694	226.75	0.3098	1678.34	2040.03	361.69	77.838	231.96
0.3198	0.0750	1.1624	1713.60	0.9052	10.944	325.34	0.4445	1682.43	2040.03	357.59	78.000	332.60
0.4051	0.0949	1.1953	1751.40	0.9252	14.444	436.87	0.5969	1696.04	2040.03	343.99	78.534	449.76
0.4904	0.1149	1.2304	1791.57	0.9464	16.694	514.66	0.7032	1716.05	2040.03	323.97	79.308	523.79
0.5756	0.1349	1.2585	1822.78	0.9629	18.194	569.15	0.7776	1731.65	2040.03	308.38	79.902	578.10
0.6609	0.1550	1.2785	1844.07	0.9741	19.444	613.87	0.8387	1738.89	2040.03	301.13	80.175	623.01
0.7462	0.1749	1.2960	1862.94	0.9841	20.594	655.29	0.8953	1743.89	2040.03	296.14	80.362	664.67
0.8315	0.1949	1.3136	1881.60	0.9940	21.844	700.12	0.9566	1746.50	2040.03	293.53	80.459	709.94
0.8827	0.2069	1.3242	1892.95	1.0000	22.594	727.28	0.9937	1747.66	2040.03	292.36	80.502	737.39
0.9040	0.2119	1.3242	1892.95	1.0000	22.744	731.85	1.0000	1745.75	2040.03	294.27	80.431	742.18
0.9296	0.2179	1.3171	1884.98	0.9957	22.844	731.80	0.9999	1737.13	2040.03	302.90	80.108	742.85
0.9552	0.2239	1.2632	1826.43	0.9648	21.694	675.15	0.9225	1697.06	2040.03	342.97	78.574	688.80

MASS AVE TOT. PRESS. 164.270
MASS AVE TOT. TEMP. 1147.084
IMP.PRESS.RATIO 5.929 TEMP.RATIO 1.736 EFF 0.890
IMP..IND.PRESS.RATIO 11.250 TEMP.RATIO 2.211 EFF 0.802 NET EFF 0.802

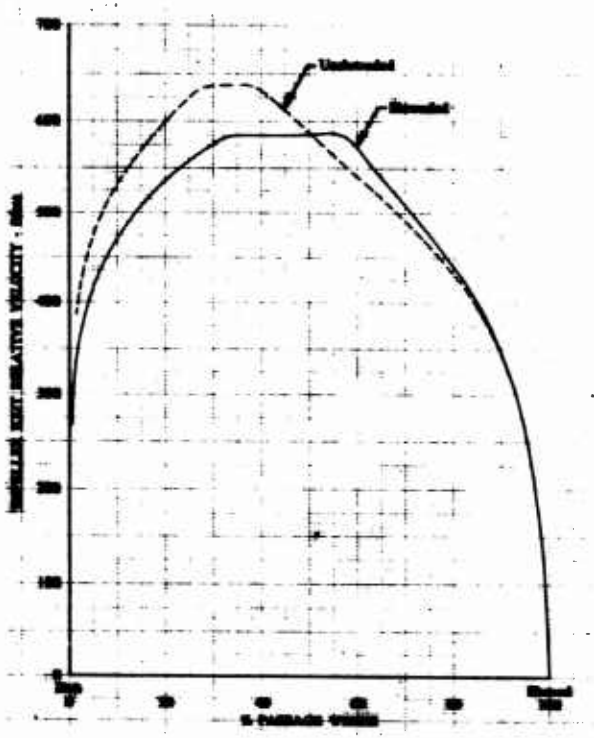

Figure 38. Comparison of Predicted Impeller Exit Relative Velocity Profile for Shrouded and Unshrouded Impellers (101% Speed, 10-deg IGV).

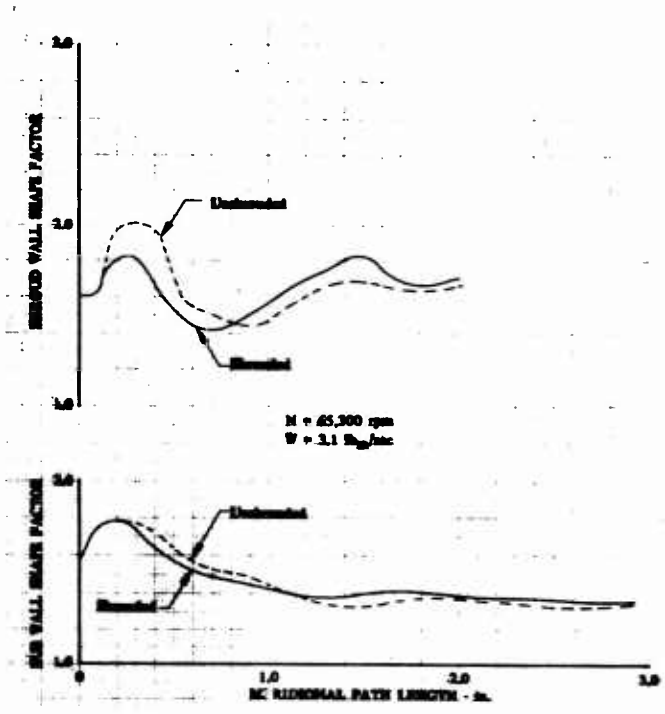

Figure 39. Comparison of Predicted Hub and Shroud Wall Boundary Layers at the Shrouded and Unshrouded Impeller Design Point.

TABLE 14. IMPELLER EXIT STATIC PRESSURE COMPARISON				
	10:1 Program		Shrouded Impeller Test	
Test Condition	Rim Static, psia	Backface Cavity, psia	Rim Static, psia	Backface Cavity, psia
101%, -4 deg IGV, near stall	54.19	55.26	51.53	56.52
101%, 0-deg IGV, near stall	53.35	54.17	50.42	55.38
101%, 0-deg IGV, minimum backpressure	52.35	53.26	50.20	54.96

The concept of the shrouded impeller was based on its reducing the impeller front face shroud friction temperature rise. The results of an analysis made to determine the magnitude of this reduction, using the impeller exit traverse data, is presented in Figure 40. This analysis indicates a reduction in shroud friction temperature rise of approximately 15 deg by using a shroud, which is about half of the predicted value of 27 deg. An error analysis was performed to determine the accuracy in calculating the shroud friction temperature rise due to precision errors in the measurements used in the calculation. As a result of this analysis, it was determined that an uncertainty in the difference in shroud friction temperature rise between the shrouded and unshrouded configurations of ±14 deg was possible. It must also be recognized that the magnitude of shroud friction temperature rise is small compared to the total work done in the compressor, and that it is determined by obtaining the difference between the total compressor temperature rise (a large number) and the Euler temperature rise (another large number); however, the data indicate a consistent reduction in shroud friction heating with a shrouded impeller at increasing design speeds.

A comparison of impeller slip factor for both the shrouded and unshrouded impellers operating at various speeds and IGV settings is shown in Figure 41. As shown, the levels of slip factor are comparable for both impeller configurations. This is somewhat surprising, in that a reduction in one-half the number of blades at the impeller exit would normally reduce slip factor. A possible explanation could be that the larger blade wake size, due to increased blade-to-blade loading, effectively reduced the passage width to that of the case with twice the number of blades. It can be rationalized that this would effectively maintain a high slip factor at the expense of increased wake losses.

Although the impeller slip factor is approximately the same for both configurations, the temperature rise at the same rotor speed is slightly less for the shrouded impeller despite an increase in rotor diameter of approximately 2.0%. (See Figure 42.) This increase in rotor diameter represents approximately 11.0 deg in temperature rise. The fact that this increase in temperature did not occur indicates that shroud friction temperature rise was reduced by a like amount. The sum of this number and the slightly lower measured temperature rise for the shrouded impeller agrees, as it should, with Figure 40.

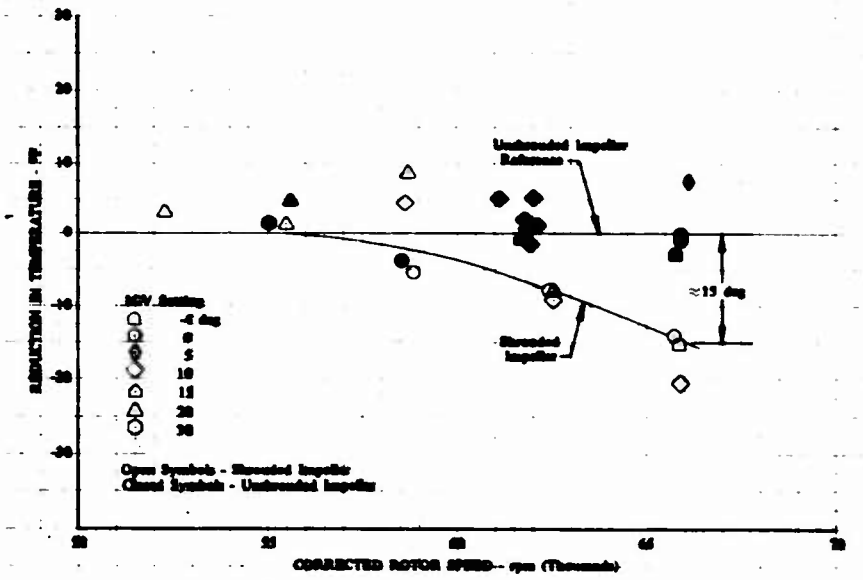

Figure 40. Reduction in Temperature Attributed to Lower Shroud Friction Heating.

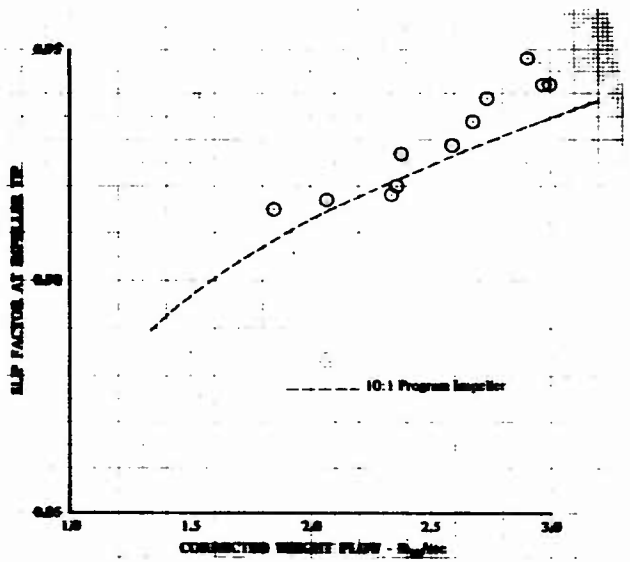

Figure 41. Shrouded Impeller Exit Slip Factor.

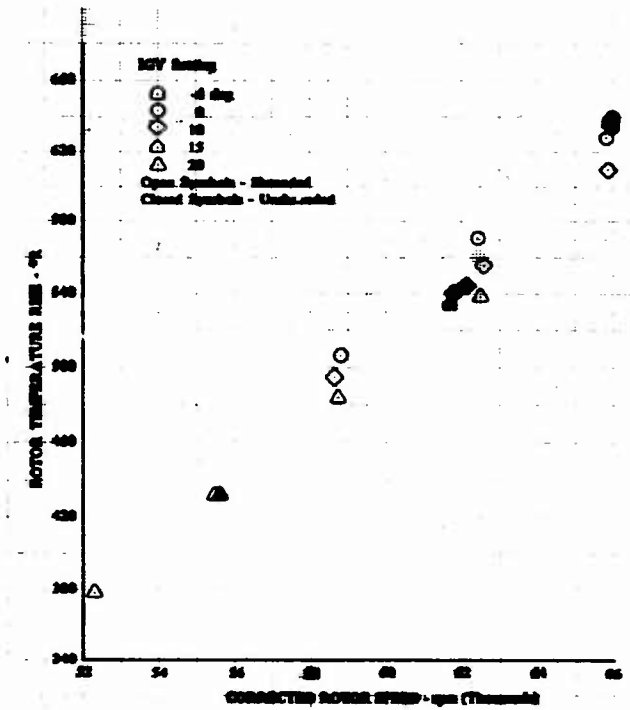

Figure 42. Comparison of Measured Compressor Temperature Rise for the Shrouded and Unshrouded Impeller Compressors.

DIFFUSER PERFORMANCE

A comparison of diffuser throat flow factor for the 10:1 program and the shrouded impeller test is shown in Figure 43 for various rotor speeds. The larger than anticipated diffuser throat blockage for the shrouded impeller diffuser effectively caused the diffuser to be undersized and resulted in a rotor/diffuser mismatch. This larger blockage can also be associated with the larger than expected diffuser losses. The diffuser total-to-total pressure losses for the shrouded impeller test are approximately 50% greater than the 10:1 program diffuser losses, as shown in Figure 44. The diffuser static pressure rise coefficient, presented in Figure 45, is also considerably reduced. This loss in diffuser performance accounts for 3.7 percentage points in overall efficiency loss at 101% speed, 0-deg IGV.

The increased diffuser throat blockage is the result of (1) increased flow blockage at the diffuser leading edge resulting from the hub wall flow separation and (2) blockage generation between the diffuser leading edge and throat associated with a diffuser leading-edge incidence variation. Although the rotating vaneless space resulted in lower wall tangential boundary layers and an improved tangential velocity profile, as shown in Figure 46, the beneficial effects that the rotating vaneless space may have had on vaneless space wall blockage were overshadowed by hub wall separation effects. Also, the hub wall separation, along with the resultant increase in flow along the shroud wall, combined to produce a larger cross channel diffuser leading-edge incidence variation, as shown in Figure 47.

Diffuser exit Mach No. profiles at near stall for 96% speed, 10-deg IGV and 101% speed, -4-deg IGV are shown in Figures 48 and 49, respectively. Corresponding profiles are given in Figures 50 and 51 for Build 6 of the 10:1 program for comparison. The high Mach No. region for the shrouded impeller test is on the hub side, while the high Mach No. region in Build 6 was on the shroud side, which directly correlates with the reversal in impeller exit profiles between the two tests.

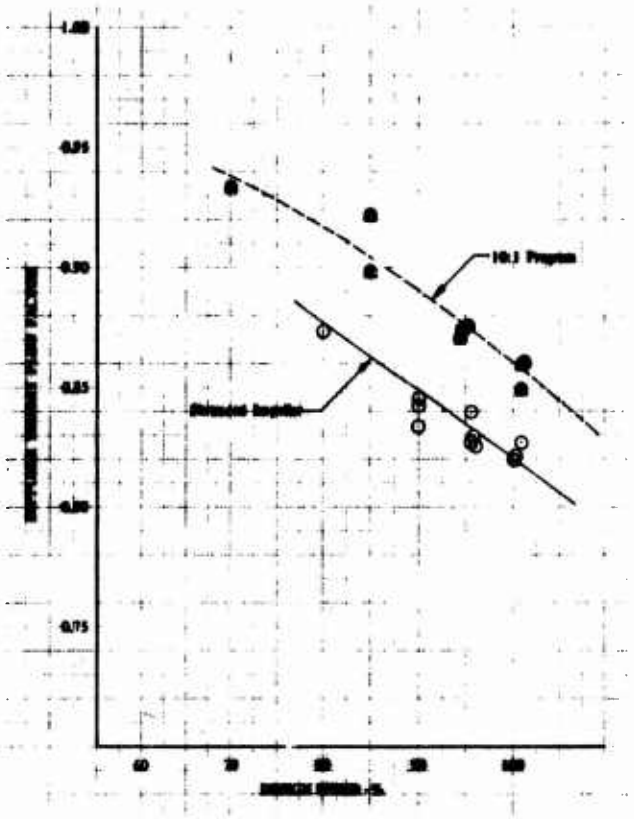

Figure 43. Comparison of Diffuser Throat Flow Factor for 10:1 Program and Shrouded Impeller Diffusers.

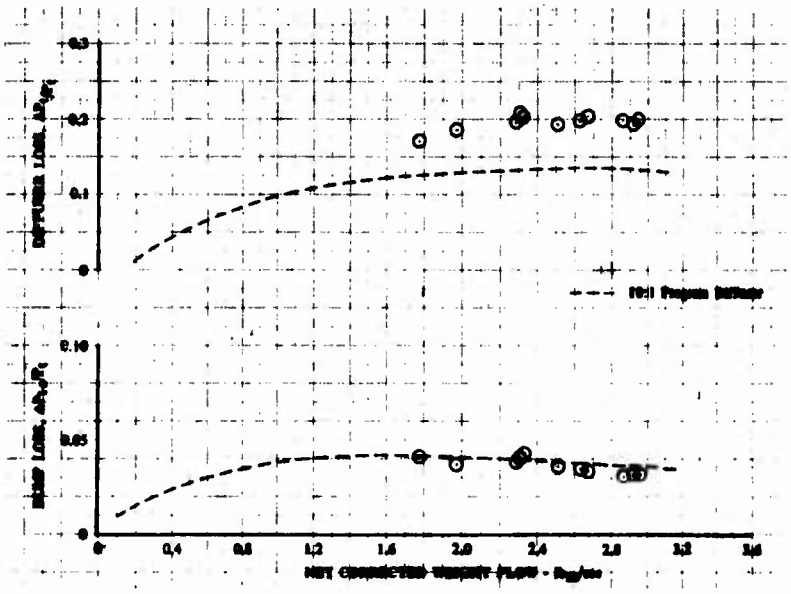

Figure 44. Shrouded Impeller Diffuser Losses.

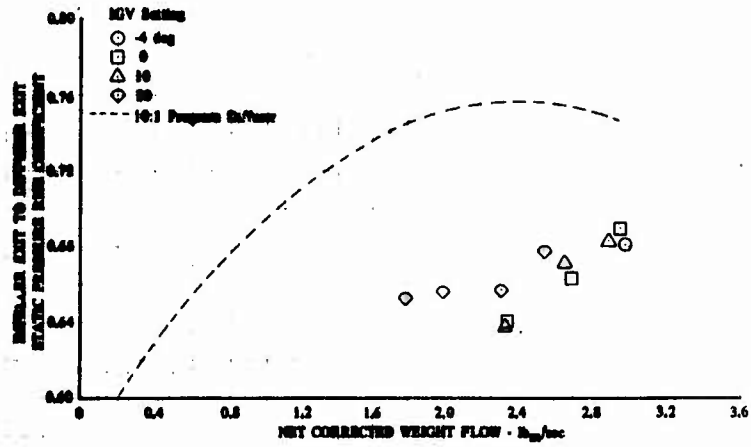

Figure 45. Shrouded Impeller Diffuser Static Pressure Rise Coefficient.

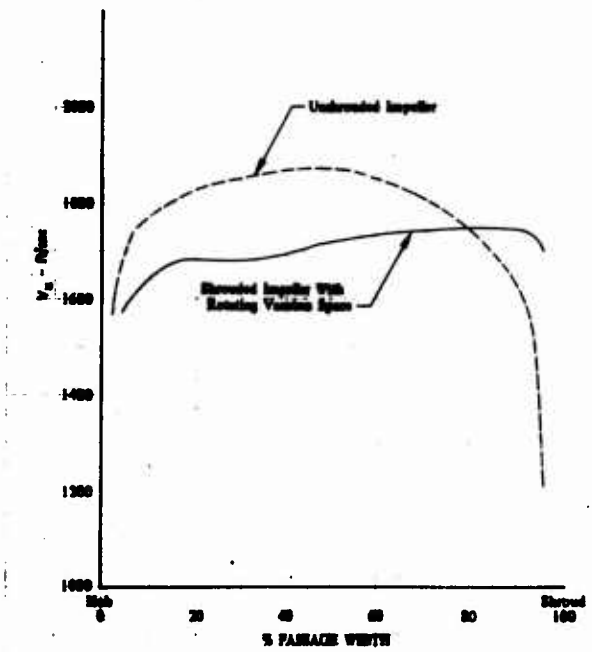

Figure 46. Comparison of Impeller Exit Absolute Tangential Velocity Profiles for Unshrouded and Shrouded Impellers (101% Speed, 0-deg IGV).

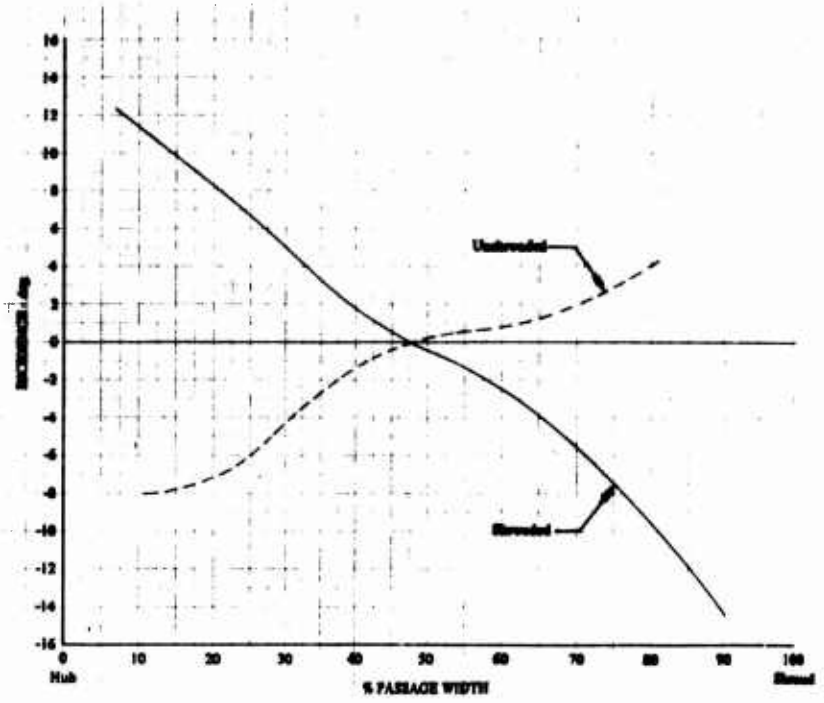

Figure 47. Comparison of Span-Wise Distribution of Diffuser Leading-Edge Incidence for the Shrouded and Unshrouded Impellers (101% Speed, -4-deg IGV).

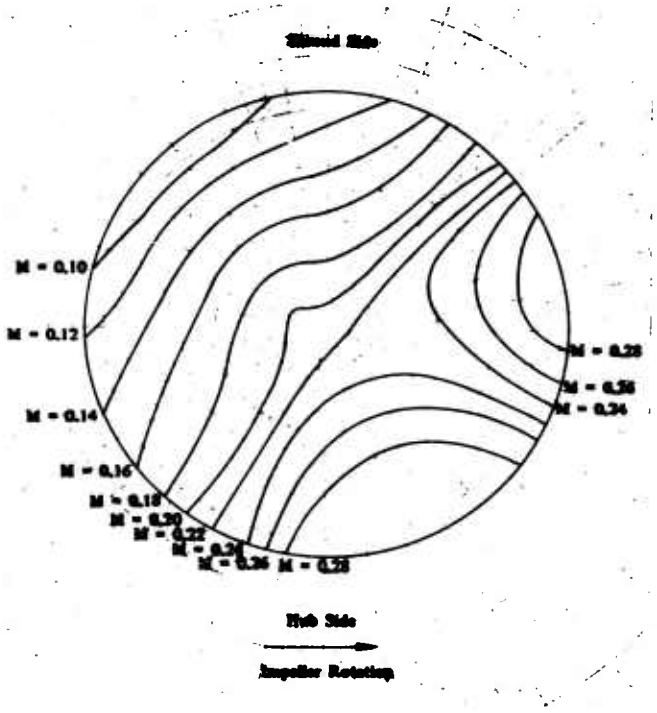

Figure 48. Shrouded Impeller Diffuser Exit Mach No. Profile (96% Speed, 10-deg IGV, Near Stall).

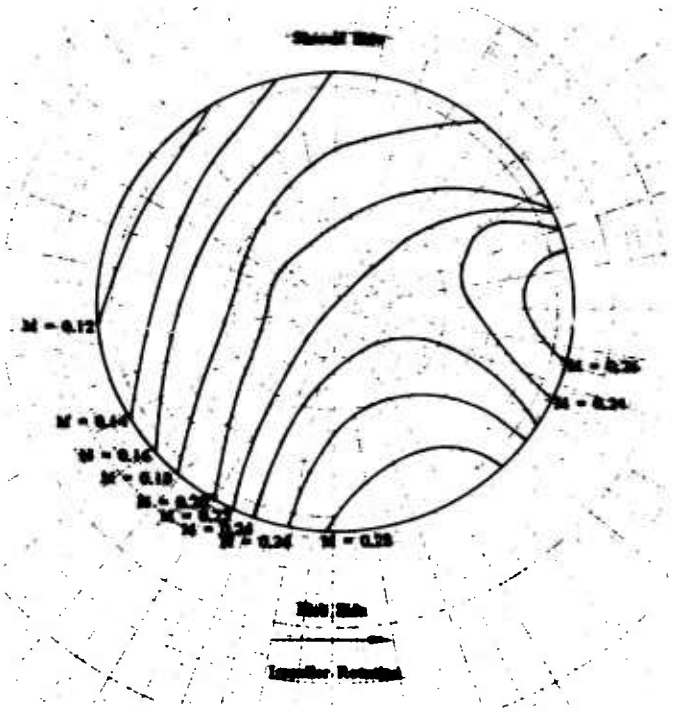

Figure 49. Shrouded Impeller Diffuser Exit Mach No. Profile (101% Speed, -4-deg IGV, Near Stall).

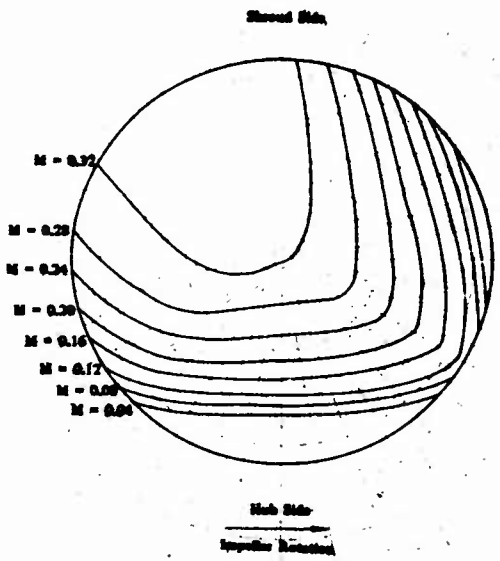

Figure 50. 10:1 Program Diffuser Exit Mach No. Profile (95% Speed, 10-deg IGV, Near Stall).

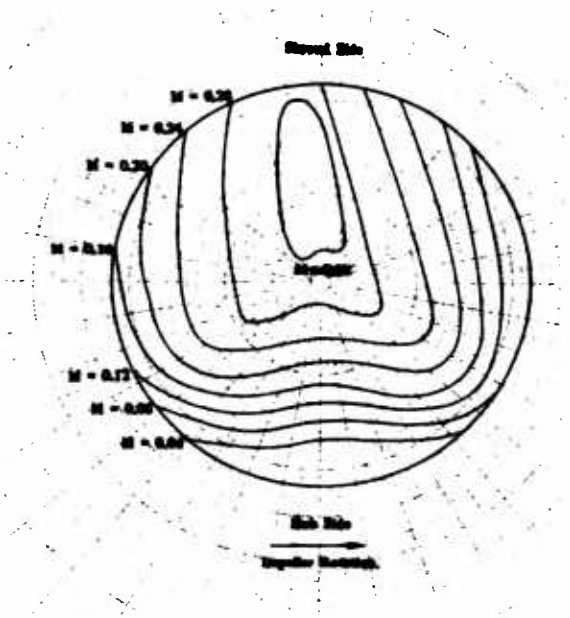

Figure 51. 10:1 Program Diffuser Exit Mach No. Profile (101% Speed, -4-deg IGV, Near Stall).

CONCLUSIONS

Based on the limited testing conducted under the program, the following conclusions are presented:

1. This program has demonstrated that it is mechanically feasible to use a shrouded impeller in a high-speed centrifugal compressor. The titanium shrouded impeller, which was machined from a single forging, was tested for 20.65 hr at tip speeds reaching in excess of 2200 ft/sec with no mechanical problems. A labyrinth seal arrangement was effectively used to limit leakage flow to less than 1% at design speed. Inspection of the rig hardware after completion of the test program revealed no damage or deformation to the shrouded impeller.

2. The design speed overall performance of the shrouded impeller compressor was 5.7 percentage points below the conventional design impeller from the 10:1 program. This poor performance was caused by higher rotor and diffuser losses and heat transfer to the fluid from cases hotter than anticipated. The higher rotor losses were attributed to an apparent flow separation at the hub wall of the impeller exit, and, to a lesser degree, the inducer operating at a stalled incidence due to a diffuser mismatch. The higher diffuser losses were attributed to excessive throat blockage due to poor impeller exit conditions, specifically the separated hub wall flow and the impeller exit air angle distribution, which caused an unfavorable incidence distribution along the diffuser leading edge. The higher case temperatures are attributed to locating the hot seal leakage flow near the impeller inlet rather than near the impeller exit.

3. The shrouded impeller did demonstrate a reduction in shroud friction heating with increasing speed, and the rotating vaneless space improved the absolute velocity profile by reducing the wall tangential boundary layers. If the apparent hub wall flow separation could be resolved, a shrouded impeller may still be able to demonstrate an improvement in performance over the original 10:1 impeller. However, the impeller analytical design system should be evaluated and improved to more accurately predict exit conditions for a shrouded impeller based on the results of this test.

RECOMMENDATIONS

Analysis of the data obtained during this program leads to the following recommendations to remedy the problems that caused the performance to be lower than predicted.

1. The design of the impeller should be improved to eliminate the severe hub wall flow separation. This separated region could be eliminated by redesigning the flow path with more convergence in the impeller exit region. This method of controlling impeller exit flow characteristics has been successfully used previously to increase the radial velocity at the shroud side of conventional impellers. The unusual hub wall flow separation should be further studied and analytical design systems improved to predict the observed effect of shrouding an impeller.

2. The impeller shroud seal should be moved from the inlet to near the impeller exit similar to the backface seals on the existing impeller. This modification would prevent heat transfer from the high-temperature impeller exit air as it circulates from the impeller tip back to the scavenge area between the seals. It would also help prevent accidental recirculation of the impeller exit air into the flow path at the impeller inlet.

3. The diffuser should be resized to match the impeller exit characteristics. The diffuser was not properly sized for the impeller exit conditions, specifically blockage and diffuser incidence, and thereby caused the performance of both the rotor and diffuser to suffer. The blockage and incidence generated at the diffuser leading edge by the shrouded impeller were considerably different from those generated by the conventional open-face impeller. The new diffuser leading-edge geometry will have to be based on the results of this report and modified based on the predicted results of converging the impeller flow path to eliminate the hub-side flow separation.

LIST OF SYMBOLS

a	speed of sound, ft/sec
A*	diffuser throat area, in^2
A	area, in^2
B	diffuser throat blockage
Cp	diffuser static pressure rise coefficient $\frac{P_{s3} - P_{s2}}{P_{t2} - P_{s2}}$
G	gravitational constant 32.174 lb_m-ft/lb_f-sec^2
e	uncertainty of an individual sensor
h	enthalpy/unit mass, Btu/lb_m
i	incidence, deg $\beta^* - \beta$
J	work constant 778 ft-lb/Btu
k	f (Mach No.) $M\sqrt{\frac{\gamma G}{R}}\left(1 + \frac{\gamma - 1}{2} M^2\right)^{-\frac{\gamma+1}{2(\gamma-1)}}$
M	absolute Mach No.
n	number of sensors
N	rotor speed, rpm
P_s	static pressure, psia
P_t	total pressure, psia
PR	pressure ratio
R	gas constant 53.345 ft, lb_f/lb_m-°R
T	total temperature, °R
T_s	static temperature, °R
TR	temperature ratio
u	overall uncertainty
U	rotor speed, ft/sec
V	absolute velocity, ft/sec

LIST OF SYMBOLS (Continued)

W	weight flow, lb_m/sec
w	relative velocity, ft/sec
α	absolute air angle, deg from tangential direction
β	relative air angle, deg from tangential direction
β^*	leading edge metal angle, deg
γ	ratio of specific heats
δ	pressure correction, $P_0/14.696$
Δ	differential
η	adiabatic efficiency
θ	temperature correction, $T_0/518.688$

Subscripts

0	plenum
1	IGV exit instrumentation station
1.5	inducer exit instrumentation station
2	impeller exit instrumentation station
3	collector
act	actual
bl	inducer bleed flow
cor	corrected to standard day inlet conditions
E	Euler
flow	flow path (not corrected for bleed and leakage flow effects)
imp	impeller
ind	inducer
m	streamline meridional component

LIST OF SYMBOLS (Continued)

Subscripts (Continued)

net	net (corrected for bleed and leakage flow effects)
o	inlet flow
sf	impeller front face shroud friction
sl	seal leakage flow
u	tangential component

Superscripts

$(\bar{})$	mass averaged